Presentation and evaluation of the Arctic sea ice forecasting system neXtSIM-F

Timothy Williams[1], Anton Korosov[1], Pierre Rampal[1], and Einar Ólason[1]

[1]Nansen Environmental and Remote Sensing Center, Thormøhlensgate 47, 5006 Bergen, Norway and the Bjerknes Center for Climate Research, Bergen, Norway

Correspondence: Timothy Williams (timothy.williams@nersc.no)

Abstract. The neXtSIM-F forecast system consists of a stand-alone sea ice model, neXtSIM, forced by the TOPAZ ocean forecast and the ECMWF atmospheric forecast, combined with daily data assimilation. It was tested for the northern winter of 2018 – 2019 with different data being assimilated and was found to perform well. Despite drift not being assimilated in our system, we obtain quite good agreement between observations, comparing well to more sophisticated coupled ice-ocean

5 forecast systems. The RMSE in drift speed is around 3 km/day for the first three days, climbing to about 4 km/day for the next day or two; computing the RMSE in the total drift adds about 1 km/day to the error in speed. The drift bias remains close to zero over the whole period from Nov 2018 – Apr 2019. The neXtSIM-F forecast system assimilates OSISAF sea ice concentration products (both SSMI and AMSR2) and SMOS sea ice thickness by modifying the initial conditions daily and adding a compensating heat flux to prevent removed ice growing back too quickly. This greatly improved the agreement of

10 these quantities with observations for the first 3 – 4 days of the forecast.

1 Introduction

Arctic sea ice has been in great decline in the last number of years (Meier, 2017). Perovich et al. (2018) report that in 2018, the summer extent was the sixth lowest and the winter extent was the second lowest in the satellite record (1979–2018). Moreover, surface air temperatures in the Arctic continued to warm at twice the rate relative to the rest of the globe, and Arctic air

15 temperatures for the past five years (2014-18) have exceeded all previous records since 1900 (Overland et al., 2018), which will also contribute to future sea ice decline if it continues.

With less sea ice comes an increase in summertime accessibility for shipping. Azzara et al. (2015) considered a range of different scenarios and projected an increase in the number of vessels operating in the Bering Strait and the U. S. Arctic of between 100 and 500%. The International Maritime Organization has also recognized that shipping would increase and adopted

20 an International Code for Ships Operating in Polar Waters (Polar Code)[1] on 1 January 2017. This polar code addresses the increased safety and pollution risks of operating in the Arctic. A recent example of the risks and comcomitant costs of accidents in the Arctic is the rescue of the fishing vessel Northguider, which ran aground between Spitzbergen and Nordaustlandet

---

[1]http://www.imo.org/en/MediaCentre/HotTopics/polar/Pages/default.aspx

(Svalbard) after getting into trouble with sea ice. The crew had to be rescued by the Norwegian Coast Guard icebreaker K.V. Svalbard, who then had to drain 300kL of diesel from the damaged vessel.[2]

Thus sea ice forecasting is becoming increasingly important. As well as search and rescue/accident prevention, other applications are optimized ship (icebreaker) routing based on forecasts (Kaleschke et al., 2016) and support of research activities – e.g. Schweiger and Zhang (2015) give an example of scheduling of high-resolution SAR images in order to follow the drift of some ice-mass balance (IMB) buoys by using the PIOMAS/MIZMAS forecast from the University of Washington. The planned year-long drift of the Polarstern from September 2019 (part of the MOSAIC project) will also rely heavily on sea ice and weather forecasts.

The sea ice forecast system neXtSIM-F is based on a stand-alone version of the sea ice model neXtSIM (Rampal et al., 2016, 2019). The dynamical core of this model is based on the Maxwell-Elasto-Brittle (MEB) rheology as developed for sea ice and originally presented in Dansereau et al. (2016), which showed its capabilities at reproducing the main spatial characteristics of sea ice mechanics and deformation: strain localization and scaling (Marsan et al., 2004; Rampal et al., 2008; Stern and Lindsay, 2009). With the implementation of this rheology in neXtSIM (along with accompanying thermodynamics and general model infrastructure: Rampal et al., 2019), MEB was able to be assessed over longer simulations, and it was found that it could also reproduce the observed temporal deformation scalings, in addition to the spatial ones. In particular, the results show strong multifractality, meaning that higher deformations are more localised in space and more intermittent in time than smaller ones. These properties have strong implications for things like distribution and size of lead openings and how long they will stay open, which will in turn have strong impacts on the heat and salt fluxes across the ocean–ice–atmosphere coupled system. Perhaps more pertinently in a forecast context, they also are highly relevant for navigation.

The paper begins by summarising the current status of sea ice forecasting in the Arctic, and then we assess the dynamical and thermodynamical behaviour of the neXtSIM model in a free run over the winter of 2018–2019. This is followed by a demonstration of the neXtSIM-F forecast system for the same winter, particularly concentrating on the benefits of two different assimilation methods: one assimilating OSISAF and AMSR2 sea ice concentration, and a second assimilating SMOS ice thickness in regions where sea ice is relatively thin, i.e. lower than 0.5 m.

2 Sea ice forecasting status

The official European forecast for the Arctic is developed and run by the CMEMS (Copernicus Marine and Environmental Monitoring Service) ARC-MFC (Arctic Marine Forecasting Centre)[3]. This uses the TOPAZ system (Simonsen et al., 2018; Sakov et al., 2012), which uses version 2.2.37 of the Hybrid Coordinate Ocean Model (HYCOM) (Bleck, 2002). In the current version (4) of TOPAZ, HYCOM is coupled to a sea ice model derived from the version 4.1 of the Community Ice CodE (CICE); ice thermodynamics are described in Drange and Simonsen (1996), while the dynamics are based on the visco-plastic (VP) sea ice rheology (implemented with the elastic-viscous-plastic (EVP) solver of Hunke and Dukowicz, 1997). The model's

---

[2]https://www.highnorthnews.com/en/svalbard-preparing-extreme-pumping-operation-using-small-boats

[3]Three institutes contribute to the ARC-MFC: the Nansen Environmental and Remote Sensing Center, the Norwegian Meteorological Institute and the Norwegian Institute for Marine Research.

native grid covers the Arctic and North Atlantic Oceans and has a horizontal resolution of between 11 and 16 km. TOPAZ4 uses the Ensemble Kalman filter method (EnKF; Sakov and Oke, 2008) to assimilate remotely sensed sea level anomalies, sea surface temperature, sea ice concentration, sea ice thickness and Lagrangian sea ice velocities (the latter two in winter only), as well as temperature and salinity profiles from Argo floats. Data assimilation is performed weekly. The most recent validation

5 report (Melsom et al., 2018), reports a bias in drift of about 2 km/day, with an RMSE of about 5–8 km/day, and a RMSE in concentration of about 0.18–0.20. The ice edge error ranged from about 30–100 km (50 km on average).

The U.S. Naval Research Laboratory runs the Global Ocean Forecast System (Metzger et al., 2017, GOFS 3.1,) which uses HYCOM 2.2.99 coupled to CICE (Community Ice CodE) on a global grid with 1/12° resolution (about 9 km). The assimilation package, NCODA (Navy Coupled Ocean Data Assimilation), uses the 3DVar method (Parrish and Derber, 1992)

10 to assimilate available satellite altimeter observations, satellite and in-situ sea surface temperature as well as in-situ vertical temperature and salinity profiles from XBTs, Argo floats and moored buoys. Surface information is projected downward into the water column using Improved Synthetic Ocean Profiles (Helber et al., 2013). In addition, a blend of ice products are assimilated: concentration from AMSR2 (Advanced Microwave Scanning Radiometer 2: Melsheimer, 2019), and extent from IMS (Interactive Multisensor Snow and Ice Mapping System: Helfrich et al., 2007) and MASIE (Multisensor Analyzed Sea

15 Ice Extent: Fetterer et al., 2010). Metzger et al. (2017) report an RMS drift speed error of about 5–8 km/day in the Arctic. This is similar to TOPAZ, although different drift products are used for the validation (IABP buoy trajectories, instead of the OSISAF high resolution ice drift) and Melsom et al. (2018) use the vector difference in their RMSE definition (which will be higher than the RMS difference between the speeds). GOFS 3.1 also showed an ice edge error of about 20-50 km (growing with forecast lead time).

20 ## 3 Data sources

3.1 Sea ice concentration from OSISAF

The Ocean and Sea Ice Satellite Application Facility (OSISAF) provides estimates of sea ice concentration derived from the Special Sensor Microwave Imager Sounder (SSMIS) radiometer (Tonboe et al., 2016; Tonboe and Lavelle, 2016; Lavelle et al., 2017) and from AMSR2 (Lavelle et al., 2016a, b; Tonboe and Lavelle, 2015). The SMMIS algorithm uses the 19 GHz frequency

25 (vertically polarized, footprint size about 56 km) and the 37 GHz frequency (both vertically and horizontally polarized, footprint size about 33 km). The AMSR2 algorithm uses three frequencies: 18.7, 36.5 and 89 GHz (also in vertical and horizontal polarizations) with footprints from 22 to 5 km). The AMSR2 data are presented on a 10-km grid, and we chose this product over the higher resolution (3.25 km) ASI product as we found it less noisy near the ice edge. These products are available daily within 12 hours after acquisition and processing so it is possible to assimilate this data in operational forecasts.

30 As specified in the validation reports above the SMMIS has lower resolution ice concentration but has the advantage of higher accuracy, while the AMSR2 algorithm has higher resolution but also higher uncertainties. In order to combine the advantages of these products we generated a blended product that was used both for assimilation and evaluation of the forecasts. Blending

was performed with a weighted average of the two products (using the errors in the products to calculate the weights):

$$C_B = \frac{C_L \sigma_L^{-2} + C_H \sigma_H^{-2}}{\sigma_H^{-2} + \sigma_L^{-2}} \tag{1}$$

where C denotes sea ice concentration, σ denotes the concentration uncertainty, index H denotes high resolution (AMSR2) and L - low resolution (SMMIS).

5   Sea ice extent, used as an evaluation metrics of the model, was calculated from the concentration product as a sum of areas of all pixels within the model domain with concentration above 15%. Sea ice extent uncertainty was calculated as a difference between the extents calculated from the sum of concentration and uncertainty and concentration alone.

3.2   Sea ice drift from OSISAF

Low resolution ice drift datasets are computed on a daily basis from aggregated maps of passive microwave (e.g. SSM/I,
10 AMSR-E) or scatterometer (e.g. ASCAT) signals (all channels are used) using the continuous maximum cross-correlation method (CMCC, Lavergne et al., 2010; Lavergne and Eastwood, 2010; Lavergne, 2010). In summer, surface melting and a denser atmosphere preclude the retrieval of meaningful information. From October to April, however, global ice drift vectors can be obtained for 48 hours at a spatial resolution of 62.5 km. To pick the most trustworthy drift vectors, we apply a threshold to the drift uncertainty of 1.25 km/day. Doing this still retains 75% of the observation vectors, with the removed ones generally
15 close to the ice edge, coast or the north pole. The error is higher in these region as the sub-images on which the CMCC method is applied must be reduced to limit them to being inside the ice mask (Lavergne and Eastwood, 2010). In the case of the north pole, there are fewer observations there, while the vectors in the MIZ have especially high uncertainties (sometimes up to 6 km/day) due to the high velocities in those regions, combined with the relatively long time interval over which the drift is calculated.

20 ## 3.3   Thin sea ice thickness from SMOS

This product from ESA's Soil Moisture and Ocean Salinity (SMOS) mission estimates the average thickness of thin ice from brightness temperatures retrieved from the low microwave frequency of 1.4 GHz (L-band) a(Kaleschke et al., 2016; Tian-Kunze et al., 2014). It uses an algorithm based on a combined thermodynamic and radiative transfer model which accounts for variations of ice temperature and ice salinity. These latter two variables are estimated using the following auxiliary data from
25 models:

- 2-m air temperature and 10-m wind velocity from the Japanese 25-year Reanalysis (JRA-25: Onogi et al., 2007).

- Sea surface salinity (which cannot be determined from SMOS under ice) is estimated from an 8-year (2002 – 2009) climatology of results from the MITgcm ice-ocean model (Marshall et al., 1997) run at a resolution of 4km and forced by the Era-Interim atmospheric reanalysis.

It also assumes the ice thickness distribution follows the one measured in NASA's IceBridge airborne campaign (Kurtz et al., 2013). Although it is distributed on a grid with a resolution of 12.5 km, SMOS has a footprint of about 40 km. It is a daily product with a delay of only $1-2$ days so it is possible to assimilate this data in a forecast situation.

Thin ice volume, used for evaluating the forecasts, was calculated by integration of ice thickness (either from observations or from the simulated fields) in all pixels with thickness below 0.5 m.

3.4 Sea ice thickness from CS2-SMOS

For long-term thickness evaluation we use the weekly hybrid CS2-SMOS product (version 2.0: Ricker et al., 2017) which combines thickness estimates from the Cryosat-2 (CS2) altimeter (more reliable for thicker ice ($\gtrsim 0.5$ m) and from SMOS (better for thin ice). The CS2 altimeter tracks are somewhat sparse so optimal interpolation (OI) is used to fill the gaps between them and the areas of thin ice. (This is also why the product is weekly and not daily.) The OI method requires a background field to be created with full coverage, and that is independent of the target week so it is created from the CS2 values for the two weeks ahead and behind the target week, and from the SMOS values for the day before the target week.

The errors from this approach can be particularly high in coastal areas of thick ice (for example north of Greenland and Canada), which are too thick to be measured by SMOS, but may be only covered by altimeter tracks every 2–3 weeks. For these gaps in coverage, the product uses the background field.

From an operational point of view, the need for the background field requires at least two weeks delay before the results for a given target week can be obtained, so it would be difficult to use this product operationally.

3.5 Forecast ocean forcing from TOPAZ4

The TOPAZ ice-ocean forecast was discussed in §2. To force neXtSIM, we use the near-surface (30 m) ocean velocity and the mixed layer depth (MLD) directly in the model, while the temperature and salinity in the model's slab ocean are relaxed towards the TOPAZ sea surface (3 m) temperature (SST) and salinity (SSS) (respectively) over a time scale of about a month. The thickness of the slab ocean is the MLD from TOPAZ.

3.6 Atmospheric forcing from ECMWF

For our forecast demonstration, we use Cycle 45r1 of the Integrated Forecast System from ECMWF (IFS: Owens and Hewson, 2018) to force neXtSIM. This is the latest version of the IFS, which came into operation in May 2018. It consists of an atmospheric model coupled to the NEMO 3.4 ocean model (Nucleus for European Modeling of the Ocean), the LIM2 (Louvain-la-neuve Sea Ice Model) sea ice model, the ECWAM (ECMWF WAve Model) wave model, and a land surface model (HTESSEL).

We use the 10-m wind velocity, the 2-m air and dew point temperatures (the latter is used to determine the specific humidity of air for the latent heat flux calculation), the mean sea level pressure, the long- and short-wave downwelling radiation, and the total precipitation (this becomes snow if the temperature is below 0°C).
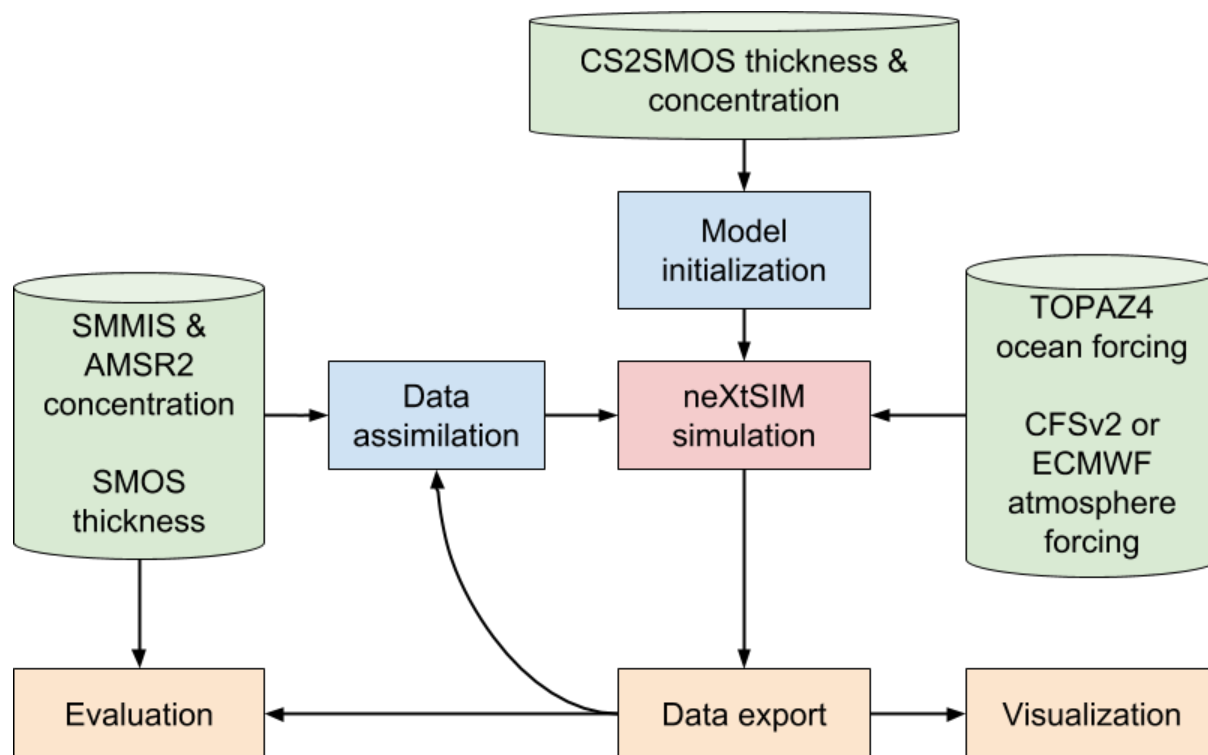
Figure 1. Overall scheme of the forecasting platform. Blue blocks contain pre-processing steps, red block - running of the model core, yellow blocks - post-processing steps, green blocks - input data.

3.7 Atmospheric reanalysis forcing from CFSv2

Due to problems with our download of the ECMWF forecast, we had to fill a gap in our atmospheric forcing of just over two weeks, from 15-29 January 2019, with reanalysis forcing. For this we use the Climate Forecast System version 2 (CFSv2, Saha et al., 2014). This is an atmospheric model coupled to the MOM4 ocean model (Modular Ocean Model, Griffies et al., 2004), which itself includes a sea-ice component. It also uses the Noah land-atmosphere model Ek et al. (2003), and the 3DVAR assimilation method (Parrish and Derber, 1992). We use the 10-m wind velocity, the 2-m air and specific humidity of air, the mean sea level pressure, the long- and short-wave downwelling radiation, the total precipitation and the fraction of this that is snowfall.

4 Description of the forecast platform

As shown in Figure 1 the platform consists of pre-processing steps (including generation of the model mesh and initialization of the forecast or assimilation of observations), running of the forecast by the neXtSIM model, and post-processing steps (including forecast evaluation, and visualisation). These steps are explained in details in the section below.
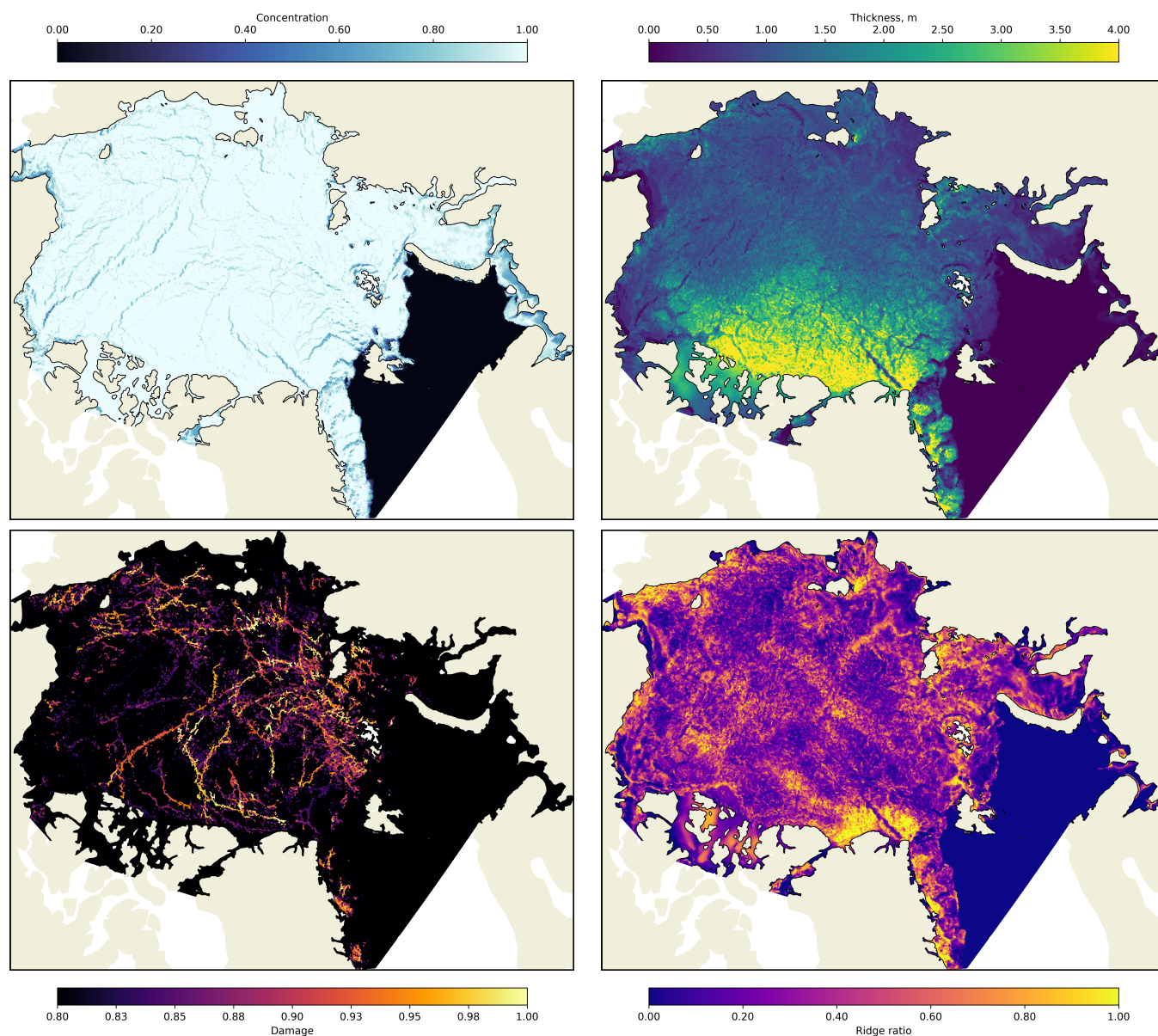
Figure 2. Example model fields from 26 February 2018 00:00: sea ice concentration; sea ice thickness; sea ice damage; ridged-ice volume ratio.

4.1 The neXtSIM model

neXtSIM is a stand-alone sea-ice model which can use winds and currents from a variety of atmospheric and oceanic models (hindcasts or forecasts). This makes it quite flexible and light to run and therefore ideal for a forecasting context. Its dynamical core is the Maxwell-elasto-brittle (MEB) rheology (Dansereau et al., 2016). Rampal et al. (2016) presented results using a

previous version of neXtSIM including an elasto-brittle (EB) rheology as described in Bouillon and Rampal (2015), showing good agreement with observed drift and concentration in particular. More recently, Rampal et al. (2019) showed the ability to reproduce the characteristic multi-fractal scalings of deformation when using the current version of neXtSIM, which now includes the MEB rheology. Rampal et al. (2019) update the paper of Rampal et al. (2016), evaluating the model's improved

5   performance when using the new MEB rheology. The key addition of the MEB rheology is a viscous dissipation of stress in areas where the ice is damaged, which restricts the velocity and particularly convergence in those areas.

The dynamical equations are solved with a finite element method on a Lagrangian (moving) triangular mesh. The code has evolved from a serial (non-parallelised) Matlab code (used by eg. Rampal et al. (2016)), to a parallelised C++ code (used by Rampal et al., 2019, and presented by Samaké et al., 2017). We use this parallelised code.

10   There is also a thermodynamic component of the code and beneath the ice is a slab ocean with three variables: temperature, salinity and thickness. The temperature and salinity are modified by the heat and salinity fluxes determined by the thermodynamical model as ice melts and freezes and as the model interacts with the atmosphere. They are relaxed towards the SST and SSS from TOPAZ over a time scale of about one month, while the thickness of the slab ocean is taken directly to be the MLD of TOPAZ. The thermodynamical model is a three-category model (detailed in Rampal et al., 2019, Appendix A): open water,

15   newly-formed ice (treated as one ice layer and one snow layer; Semtner, 1976) and older ice (treated as two ice layers and a snow layer; Winton, 2000).

The older ice is characterised in the model by concentration, c, and thickness averaged over the entire cell (effective thickness or, in other words, volume per unit area), h. The absolute thickness of ice can be computed as the ratio: $H = h/c$; there is also an effective snow thickness, s. The young ice has concentration c_y, effective and absolute thicknesses, h_y and $H_y = h_y/c_y$,

20   and snow thickness, s_y. H_y is constrained so that $H_{\min} \leq H_y \leq H_{\max}$. If $H_y < H_{\min}$, c_y is reduced to $c'_y = (H_y c_y)/H_{\min}$; if $H_y > H_{\max}$, some ice is moved to the older ice category. During this process H_y is reduced to $H'_y = H_{\max}$, while c_y is also reduced to $c'_y = c_y(H_{\max} - H_{\min})/(H_y - H_{\min})$. This concentration reduction is intended to give some lateral decrease in thin ice volume and not just vertical. The corrected values for h_y and s_y are $h'_y = c'_y H_{\max}$ and $s'_y = c'_y(s_y/c_y)$; the corresponding properties for the older ice h, c and s are then increased in a ice-and-snow-volume-conserving manner. The values that we used

25   for the thresholds on the absolute thin ice thickness are $H_{\min} = 0.05\,\mathrm{m}$ and $H_{\max} = 0.275\,\mathrm{m}$.

The domain we present simulations for is a pan-Arctic one, with a resolution of about 7.5 km. A 7-day forecast for this domain can be run on a laptop with 8 cores at 2 GHz in about $3-4$ hours. Figure 2 shows snapshots of some of the more interesting variables from neXtSIM. Figure 2a shows the sea ice concentration — note the many thin cracks and leads — while Figure 2b shows the ice thickness. Figure 2c shows the damage, which is a crucial variable in the MEB rheology. The effective

30   elastic modulus is lower where it is higher, making it more mobile in those places. Figure 2d shows the volume fraction of ridged ice, which is higher in places that have been under convergence. This variable is one that could be particularly useful for icebreakers wishing to travel into the ice.

4.2 Initialization of the model fields

Before the model can be run it has to be initialized - the triangular mesh for the destination domain should be generated and initial values of sea ice concentration and thickness and the slab ocean surface temperature and salinity have to be set. The mesh is generated with Unref (a component of Gmsh: Geuzaine and Remacle, 2009) and using the Global Self-consistent, Hierarchical, High-resolution Shoreline Database (GSHHS) (Wessel and Smith, 1996). The model fields are initialized from the observed sea ice concentration and thickness from the CS2SMOS product (sec. 3.4) and simulated sea surface temperature and salinity from TOPAZ4 (sec. 3.5). The ice concentration in the CS2SMOS product is originating from the OSISAF low resolution product and has to be adjusted in areas with low thickness (Ivanova et al., 2015). Therefore total sea ice concentration (c_t) is calculated by adjusting the observed SIC using the observational operator $\mathcal{O}$:

$$
c_t = c_O / \mathcal{O}(h_{C2S})
$$
$$
\mathcal{O}(h_{C2S}) = a_0 \sinh\left(\frac{h_{C2S} - a_1 a_2}{2a_1}\right)
\tag{2}
$$

where c_O is the OSISAF concentration, h_{C2S} is the CS2SMOS (effective) thickness, and $a_0 = 0.9569$, $a_1 = 0.06787$ and $a_2 = 0.4255$ are parameters fitted from the observations (personal communication with Thomas Lavergne).

As mentioned above the model has two ice categories - young ice and older ice with different rheological behaviour. At the initialization step young ice c_y is set to comprise 20% and the older ice c 80% of the total SIC. If the observed absolute thickness h_{C2S}/c_t is below the young ice upper thickness limit $H_{\max}$, then thickness is distributed between young and older ice in the same proportion, otherwise young ice thickness is calculated as $h_y = c_y H_{\max}$ and for the older ice: $h = h_{C2S} - h_y$. It was identified that the model has little sensitivity to the fraction of young ice and it may vary within 5 - 30%.

The temperature and salinity of the slab ocean is taken to be equal to the TOPAZ4 surface forecast.

4.3 Assimilation of concentration and thickness

The assimilation is performed before each forecast run using the data insertion method — an updated variable (V_U) is calculated as a function of the forecast variable (V_F) and observations (V_O): $V_U = f(V_F, V_O)$. The simulation is then restarted using the updated variable V_U and the model is run for 7 days to provide a forecast. The assimilation is performed on the model mesh — the satellite observations, originally provided on a regular grid, are linearly interpolated onto the centers of the mesh elements so that they can be directly compared with the neXtSIM prognostic variables.

Two types of satellite observations are assimilated in neXtSIM-F: the blended concentration from OSI-SAF (c_O, sec. 3.1) and effective thickness from SMOS (h_S, sec. 3.3) using a weighted average approach:

$$
V_U = \frac{V_F \sigma_F^{-2} + V_O \sigma_O^{-2}}{\sigma_O^{-2} + \sigma_F^{-2}},
\tag{3}
$$

where V denotes ice concentration or thickness, σ denotes uncertainty of concentration or thickness, index F denotes forecast variable or uncertainty and index O - the observed ones.

The Cryosphere

Discussions

Open Access

EGU

The uncertainties of the observed concentration and thickness (σ_O^c and σ_O^h) are obtained from the input product and uncertainties of the forecast concentration and thickness (σ_F^c, σ_F^h) are set, respectively to 10% and 0.1 m. The values for the uncertainties in the forecast variables are chosen to reduce strong discontinuities in the modelled fields. Assimilation of both concentration and thickness is performed in all elements that have valid observations. Even if h_O exceeds the theoretically

5 retrievable threshold of 0.5 m the value of σ_O^h in such elements is considerably larger than σ_F^h and, thus SMOS observations have almost no impact on the updated thickness.

After calculating the updated variables as specified in (3) the fractions and thicknesses of young and older ice are calculated in the same way as in the initialisation procedure (see sec. 4.2).

Once all the assimilation steps have been performed the model fields are checked for consistency with each other and cor-

10 rected if necessary. First, the concentration of young ice is reduced in the elements where the total concentration exceeds 100%. Second, the surface temperature of the slab ocean is set to the freezing point where new ice was added during assimilation. The volume of ridged ice, damage and the snow thickness are set to zero in the added ice.

4.4 Compensating heat flux

One of the side effects of assimilation is that the heat balance in the model is disturbed: reducing the concentration opens more

15 water and given the temperatures, atmosphere humidity and ocean salinity provided by the forcing, the heat flux out of the ocean increases and the ice freezes up again very fast. A compensating heat flux is added to the total ocean heat flux in order to keep the heat balance and prevent refreezing of ice where it was removed by assimilation, thus prolonging the effect of assimilation. If c_t and c_t' are respectively the total concentrations before and after assimilation, a compensating heat flux (Q_c) is calculated if ice was removed — i.e. if $c_t > 0$ and $c_t' < c_t$ — according to the following formula

20 $$Q_c = Q_o\big((c_t'/c_t)^n - 1\big) \qquad (4)$$

where Q_o is the total heat flux from the ocean (sum of flux from the ocean to sea ice and to the atmosphere), and n is a parameter controlling the strength of correction. The function was chosen so that Q_c is zero when the concentration update is zero, and $Q_c = -Q_o$ when $c_t' = 0$, i.e. all the ice was removed by assimilation. With $n = 1$ the reduction of Q_c from 0 to $-Q_o$ is linear and with $n > 1$ it becomes steeper for values of c_t' closer to c_t. We use $n = 4$ for the runs presented here, as this gives

25 a suitably strong heat flux for a modest reduction in concentration.

5 Results

5.1 Evaluation of free model run

In this section we demonstrate that the model is generally able to reproduce the overall drift, concentration, and thickness patterns in observations of these variables. For all comparisons we average the model fields in time over an appropriate time

30 window (in practice 1, 2 or 7 days), apply some spatial smoothing (being guided by the size of the satellite footprint), and interpolate onto the observation grid. For scalar variables, we define bias as $\langle V_{\mathrm{mod}} - V_{\mathrm{obs}}\rangle$ (with $\langle \cdot \rangle$ defining the spatial mean

over pixels where both model and observation are defined.) We also define RMSE as $\langle (V_{\mathrm{mod}} - V_{\mathrm{obs}})^2 \rangle^{1/2}$. For the ice velocity we define the bias and RMSE as the mean and RMS values of the difference in speed respectively — i.e. $\langle |\boldsymbol{u}_{\mathrm{mod}}| - |\boldsymbol{u}_{\mathrm{obs}}| \rangle$ and $\langle (|\boldsymbol{u}_{\mathrm{mod}}| - |\boldsymbol{u}_{\mathrm{obs}}|)^2 \rangle^{1/2}$. We also define the vector RMSE (VRMSE), as the RMS of the vector difference, $\langle |\boldsymbol{u}_{\mathrm{mod}} - \boldsymbol{u}_{\mathrm{obs}}|^2 \rangle^{1/2}$.
For the ice extent, we use the terms bias and RMSE a bit loosely: we define bias in extent as $A_{10} - A_{01}$, where A_{10} is the

5 total area of pixels where neXtSIM predicts the presence of ice (total concentration greater than 15 %) but the observation has no ice, while A_{01} is the total area of pixels where neXtSIM predicts the no ice (total concentration greater than 15 %) but the observation does have ice; we define RMSE in extent as $A_{10} + A_{01}$. Thus the RMSE is always positive, and the bias is positive if neXtSIM is overestimating the total extent and negative if it is underestimating it. This definition of the RMSE for extent corresponds to the "Integrated Ice Edge Error" metric of Goessling and Jung (2018) for a deterministic forecast.

10 Figure 3 compares the mean concentration from neXtSIM and the OSISAF concentration product (see 3.1). Two-monthly averages values for the errors are plotted as dotted lines and are also shown in Table 1. The bias is initially oscillating about zero, but this drops around the start of March to about -2.5 %. Towards the end of April, however, a significant low bias has developed. However, the bias is mostly well within the level of the observational errors. The RMSE is generally within the error range, but like the bias, it starts to leave it around the end of April.

Table 1. Accuracy of the free run. Concentration and extent are evaluated against OSISAF SSMI; thickness is evaluated against CS2-SMOS; drift against OSISAF drift. Results are averaged over three periods: November – December, January – February and March – April or just March (CS2-SMOS ice thickness is not available in April).

	Concentration, %		Extent, $10^6\mathrm{km}^2$		Thickness, m		Drift, km/day		
	Bias	RMSE	Bias	RMSE	Bias	RMSE	Bias	RMSE	VRMSE
Nov-Dec	0.14	5.83	-0.02	0.23	-0.12	0.26	-0.06	2.74	4.05
Jan-Feb	-0.26	4.73	0.04	0.16	-0.01	0.35	0.25	2.52	3.58
Mar-(Apr)	-2.52	6.05	-0.10	0.21	-0.06	0.53	0.39	2.59	3.49

15 Figure 4 shows the spatial distribution of the concentration bias. There are some prominent regions of overestimation in ice extent, primarily located in the Greenland Sea, and the Barents Seas. Particularly persistent are the areas north of Novaya Zemlya (around the Santa Anna Trough), around Franz Josef land, and northwest of Svalbard. However, the area northwest of Svalbard starts to become underestimated around mid-February.

The map for Nov-Dec shows strong underestimation in the Bering Sea, which was too slow to freeze up in November, and

20 north of the Novo Sibirski Islands. This is strongest from about 3 – 11 Nov. It also returns at the start of April, although the region extends further in this period than at the start of the winter, following the Siberian coast around to the Severny Islands. There are also significant underestimations at the end of the simulation along the coasts of the Beaufort Sea (particularly Mackenzie Bay), and the Bering and East Siberian Seas. In addition, the ice off Greenland is being driven away from the coast too much, leading to a double penalty in the RMSE score at the end of the simulation.

25 Figure 5 shows time series of thickness errors when compared to CS2-SMOS, while Figure 6 also shows the spatial distribution of the errors. Also refer to Table 1 for the two-monthly averages and the average for March. Since our run was initialised
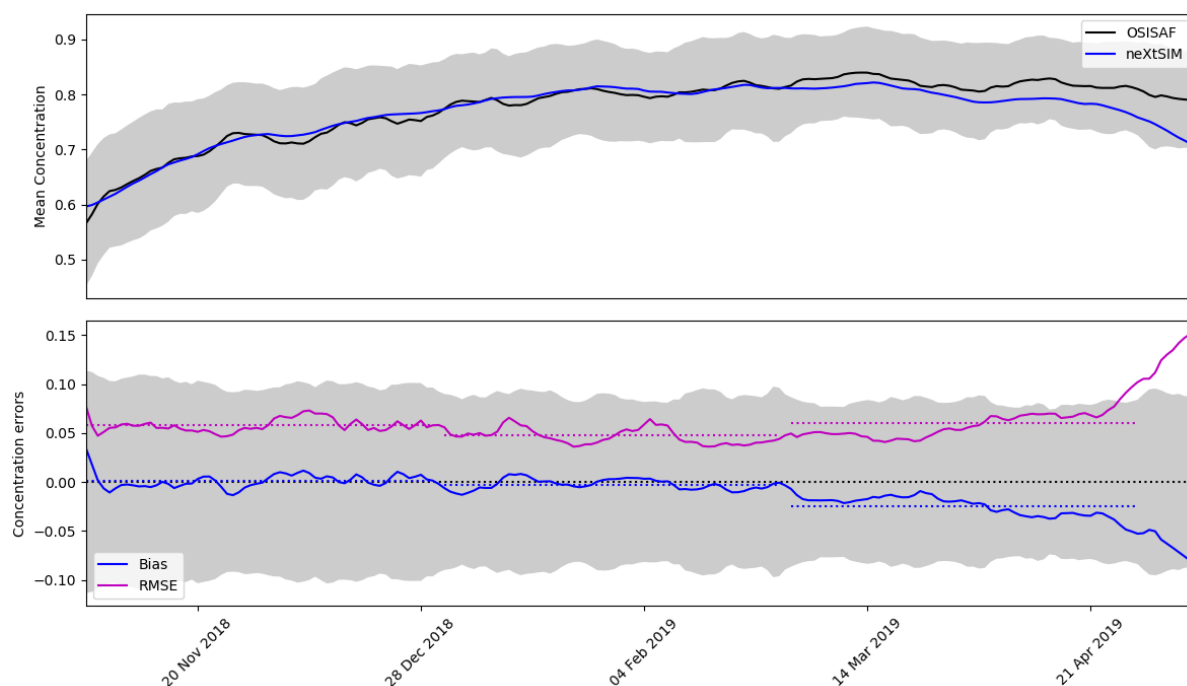
Figure 3. Temporal comparison of model and OSISAF concentrations. Two-monthly average values of the different errors are plotted as dotted lines with colours corresponding to the solid lines; these values can be found in Table 1.
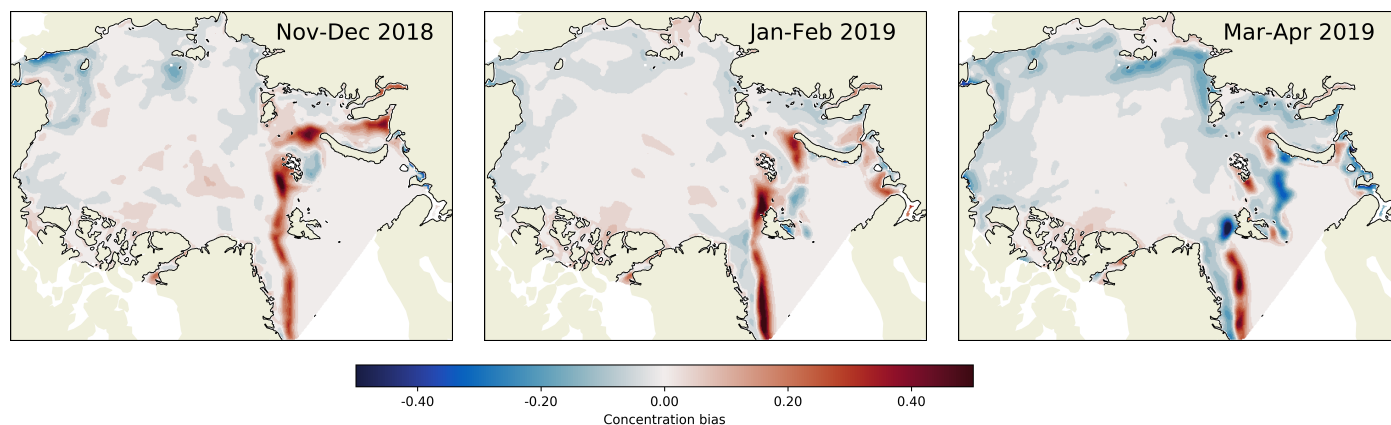

Figure 4. Spatial comparisons of 2-monthly averaged model and OSISAF concentration.

from this product, the RMSE begins well within the observation error levels, but it grows steadily over the winter, leaving the shaded area in mid-December. We note here that the error levels in the CS2-SMOS product are only the interpolation error, and are thus a lower bound as they don't include uncertainties in the individual CS2 and SMOS products. CS2 in particular is sensitive to the ice and snow densities used or the snow thickness which affect the conversion from freeboard to thickness

5 (Zygmuntowska et al., 2014).

To a large degree, this growth in RMSE is a consequence of misplacement of the ice edge. However there seems to be systematic underestimation in the central Arctic, and overestimation to the north of Greenland. More local differences are seen around Banks Island off Canada. In at least one case (26 Nov – 3 Dec 2018), this is due to opening to the north and east of Banks Island (seen in Sentinel-1 SAR images), which was captured by the model but which occurred in between CS2 altimeter

10 passes. Since the ice around there was too thick for SMOS to be reliable, this opening was not present in the CS2-SMOS product that week. Therefore it is likely that the RMSE at the start of winter is being overestimated due to cases like this where relatively thick ice in regions of infrequent CS2 coverage is still quite mobile.

The thickness bias begins slightly negative, but increases to a plateau near zero after about 2 months, remaining around there for the rest of the simulation. While it is encouraging that the mean thickness in the model (roughly total volume in domain

15 divided by total area) is approximately the same as for the observations, the growing underestimation in the central Arctic must be compensating for overestimation elsewhere. We will discuss this further in the context of the drift results below, noting that the interpolation error of CS2-SMOS is also quite high in the central Arctic.

Figure 7 shows the drift bias and RMSE of neXtSIM when compared to the OSISAF drift product. The two-monthly averages are plotted as dotted lines and are also shown in Table 1. The bias fluctuates somewhat, but stays largely within the error limits

20 of just over ± 1 km/day. The RMSE in speed is very good, averaging about 2.7 km/day for the whole winter with a maximum of about 4.5 km/day. The VRMSE (vector RMSE) for the drift is higher than the bias, RMSE and the observation error, since it also includes errors in direction, but it is still quite low, ranging from about 3-5.5 km/day. It is highest in November-December, averaging 4.1 km/day, dropping to an average of about 3.6 km/day for January-February, and then to about 3.5 km/day for March-April.

25 Figure 8 shows the general spatial pattern in the errors: drift is too slow in Mackenzie Bay and towards the Alaskan coast of the Beaufort Sea, and too fast in the MIZ and where the ice is thinner, especially the Laptev Sea. Note the bias maps are slightly eroded (near the ice edge, coast, and the north pole — see the discussion in §3.2) compared to the ice mask since we have not used observations with errors higher than 1.25 km/day. In November – December, the averaged drift map for the OSISAF product shows a reasonably strong Beaufort Gyre but which is centred nearly in line with the Bering Strait. There is

30 a strong eastward current in the East Siberian Sea and a quite wide trans-polar drift which extends over to Severnaya Zemlya and the Franz Josef Islands, although it is more connected to the Laptev Sea than the Bering Sea. These latter two features are mostly captured by the model, but it is not quite capturing the full Beaufort Gyre. This may be partly due to too much land-fast off Canada. With the exception of around the Beaufort Gyre and the Canadian Archipelago, the directional bias is quite low.

In January – February, the Beaufort Gyre is more concentrated in the Beaufort Sea, while the transpolar drift is extending

35 across the entire Arctic from the Bering Sea. There is also an anticyclonic pattern in the Laptev Sea, centered close to Severnaya
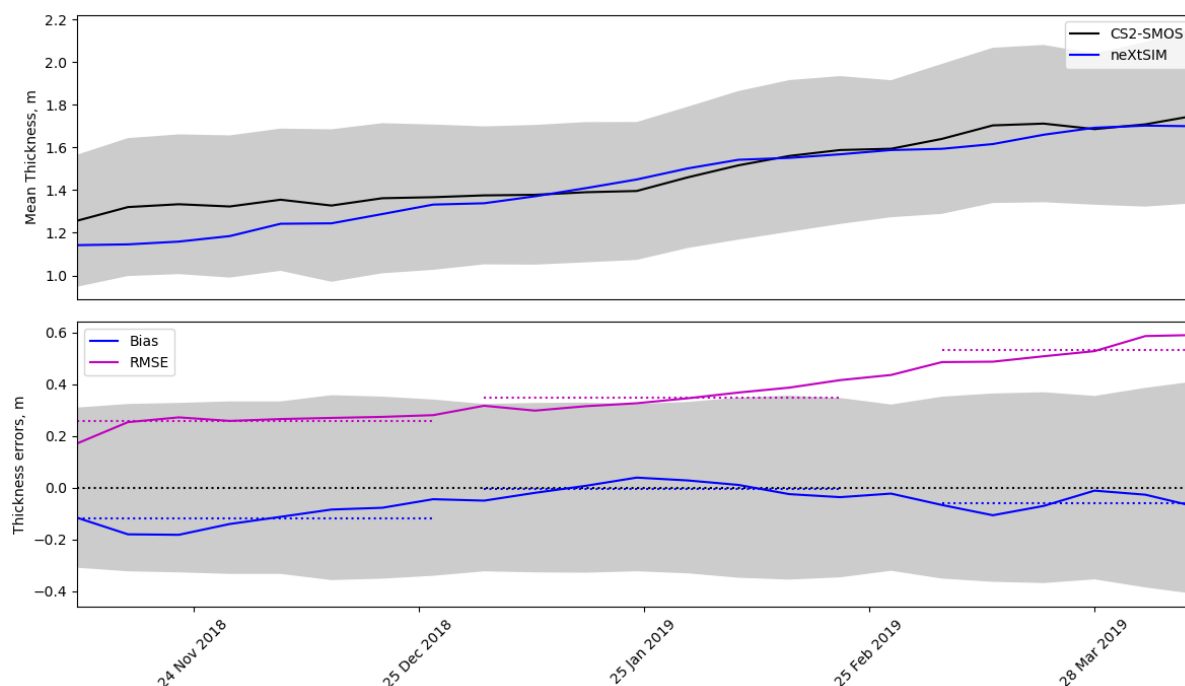
Figure 5. Comparison of model and CS2-SMOS thickness. The shaded regions show the RMS uncertainty in the CS2-SMOS product.

Zemlya. The model is capturing this behaviour quite well, reflecting the drop in VRMSE to a very respectable 3.6 km/day for this period, but it is again missing the coastal part of the Beaufort Gyre. The model direction has much improved from November – December, with most of the arrows in the bias map pointing up — this probably explains the drop in VRMSE from the first analysis period.

5   For the March – April period, the drift pattern is more like that of November – December, although there are fewer valid drift vectors. The VRMSE for this period is now about 3.5 km/day, and the model drift pattern is quite close to that of the OSISAF product (including the full Beaufort Gyre this time). The directional bias is again relatively low, but is not quite as good as for the January – February period.

5.2 Evaluation of forecasts with assimilation

10   The impact of assimilation on the forecasting skills of the model was tested in two experiments. First, we ran a single, 7-day forecast without assimilation, with assimilation of concentration and with assimilation of concentration and thickness. Second, the model was run for 6 months with daily assimilation of concentration and thickness. In this experiment, in order to reduce computation time, the 7-day forecasts were launched only every three days with 1-day forecasts being launched in between so that assimilation was still performed daily.
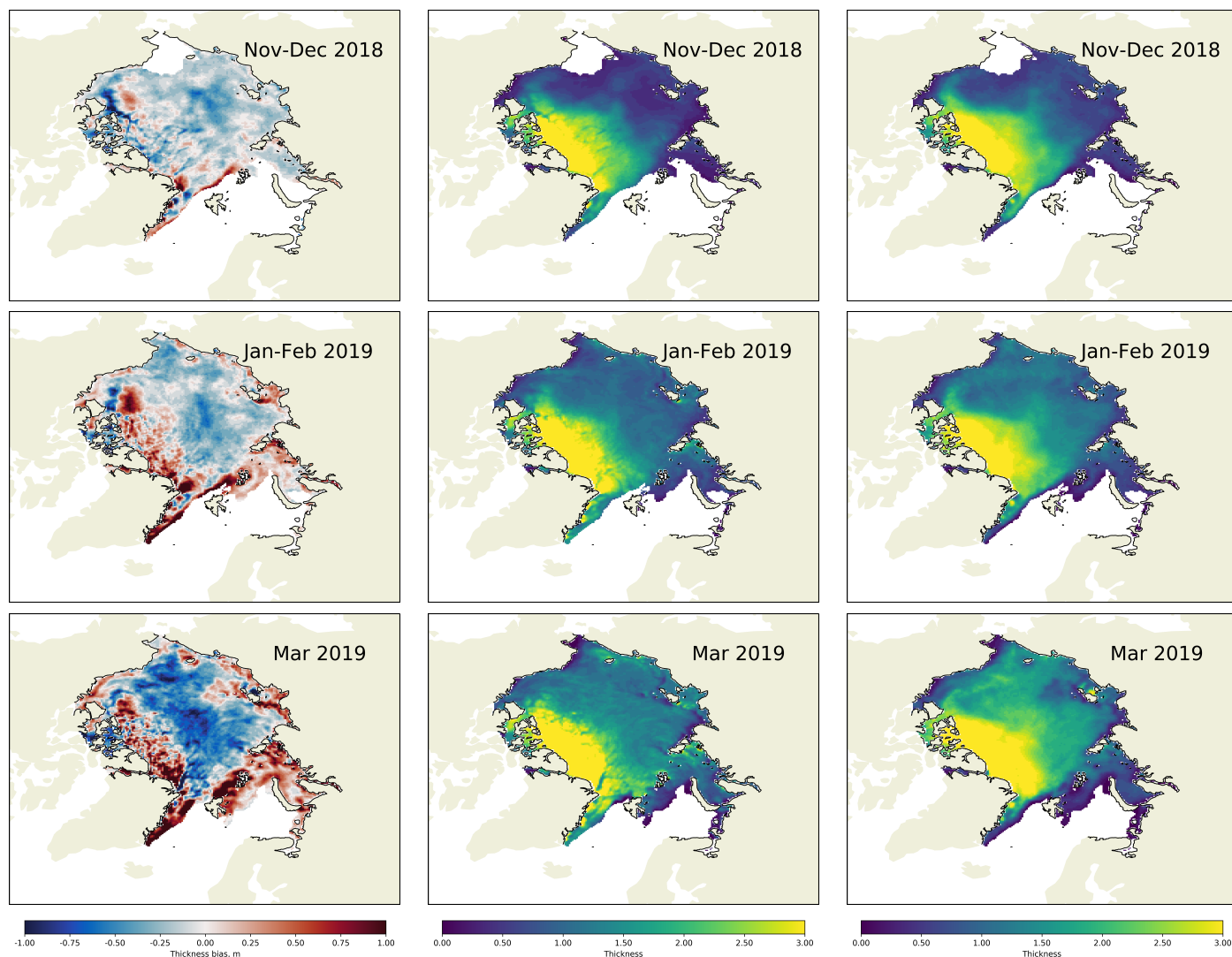
14

Figure 6. Comparisons of 2-monthly averaged model and CS2-SMOS thickness. Left hand column: bias maps; centre column: neXtSIM thickness; right hand column: CS2-SMOS thickness.
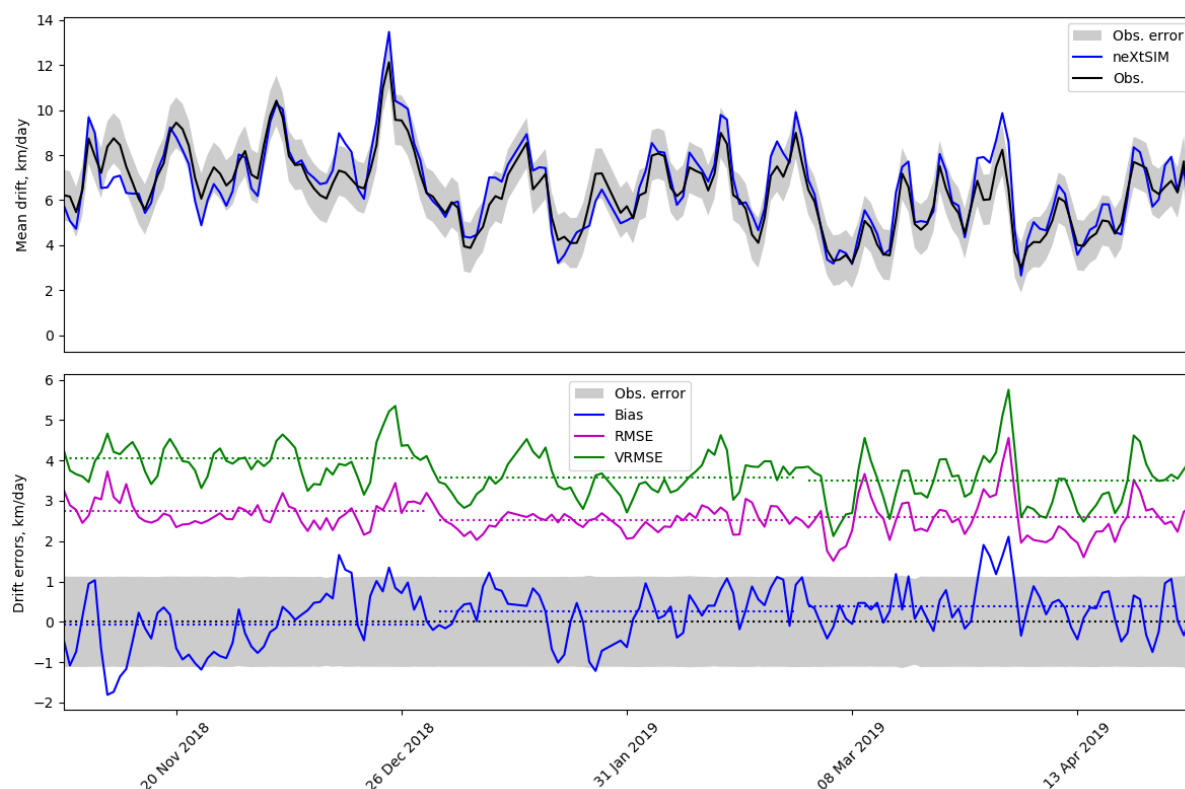
The Cryosphere
Discussions

EGU

Figure 7. Comparison of model and OSISAF drift. The shaded region shows the RMS uncertainty in the OSISAF drift product.

The model performance was evaluated against satellite observations of the blended sea ice concentration and sea ice extent from OSISAF (see sec. 3.1) and SMOS thickness (see sec. 3.3). The bias and RMSE of the forecast sea ice fields were compared with the bias and RMSE of the field averaged over the first day. In the first experiment only errors from a single 7-day forecast (starting on 7 Nov 2018) were evaluated; in the second one time series of observed and forecast variables were plotted and analyzed.

The evaluation shows that even without assimilation the model predictions of ice extent and thickness (orange lines on fig. 9) are better than the persistence fields (blue lines on fig. 9). Assimilation of concentration only (shown by green lines) reduces RMSE and bias for both concentration and thickness compared to the run without assimilation. Assimilation of thickness (red lines) has a smaller impact on the concentration forecast but significantly reduces the RMSE of the thickness. The bias in the forecast concentration and thickness is greatly reduced by the assimilation and stays closer to zero than the bias in the persistence forecast. The errors in the forecast are less than errors in the persistence forecast not only at the day of assimilation (shown by red arrow) but also for the entire 7-day run.

Figures 10 and 11 show the maps of bias in concentration and thickness for the first day (4 Nov. 2018) and the second day (5 Nov. 2018) after the assimilation, respectively. Running the model even without assimilation helps to reduce large negative
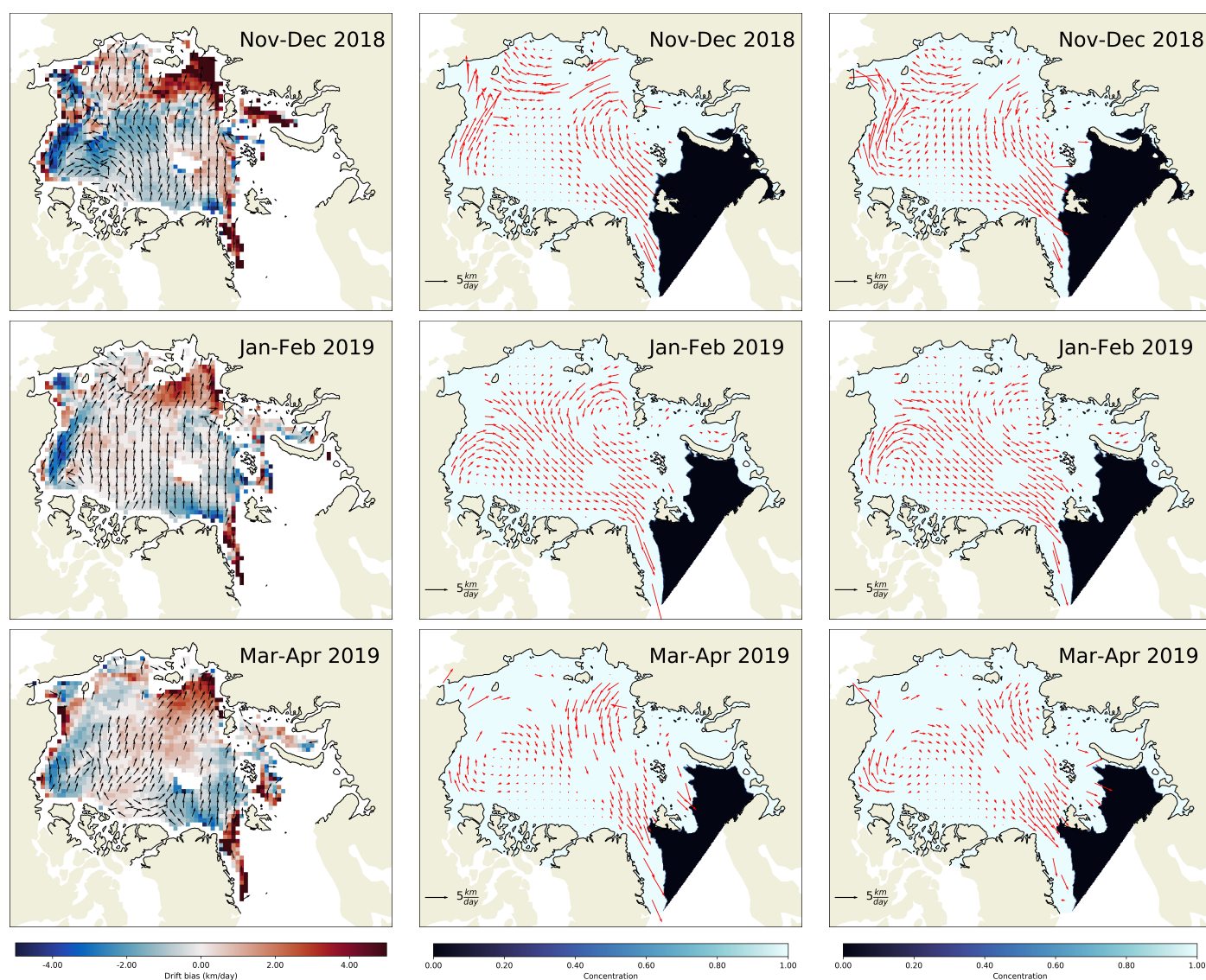
Figure 8. Comparisons of 2-monthly averaged model and OSISAF drift. The drift bias colour maps (left column) show the bias in speed, while the directions show the difference between the model and observation directions (arrows pointing up indicate the directions are the same). The central column shows ice velocity vectors from neXtSIM, while the right hand column shows OSISAF vectors. The concentration colour maps show the average neXtSIM concentration over the analysis period to indicate the approximate ice mask.

Figure 9. Evolution of RMSE (left column) and bias (right column) of persistence (blue line), forecast without assimilation (orange), forecast with assimilation of SIC only (red) and forecast with assimilation of SIC and SIT. Upper row of plots show errors in sea ice extent and the lower row - in thin ice thickness. The red arrows show the step at which assimilation was performed.

bias in concentration in the East Siberian and Chukchi seas. Assimilation of concentration helps to reduce this bias. The impact is evidently pronounced during the first day in both correcting average concentrations in the pack ice (e.g. in the Kara sea) and adjusting the ice edge position (e.g. in the Fram strait and Barents sea). Assimilation of thickness improves thin ice fields (e.g. in the Laptev). After 2 days the impact of assimilation is less pronounced (see Figure 11), however it is obvious that the errors

5 in concentration, thickness and ice edge position are still smaller than those from the persistence field and the fields from the free run.

Figure 12 shows time series of mean quantities from the second experiment with assimilation, while Figures 13, 14, and 15 present maps of bias averaged over the full period. Tables 2 and 3 summarise the average errors from this experiment. They indicate that concentration, extent, thin ice thickness and drift are consistently well predicted. The 7-day forecasts of
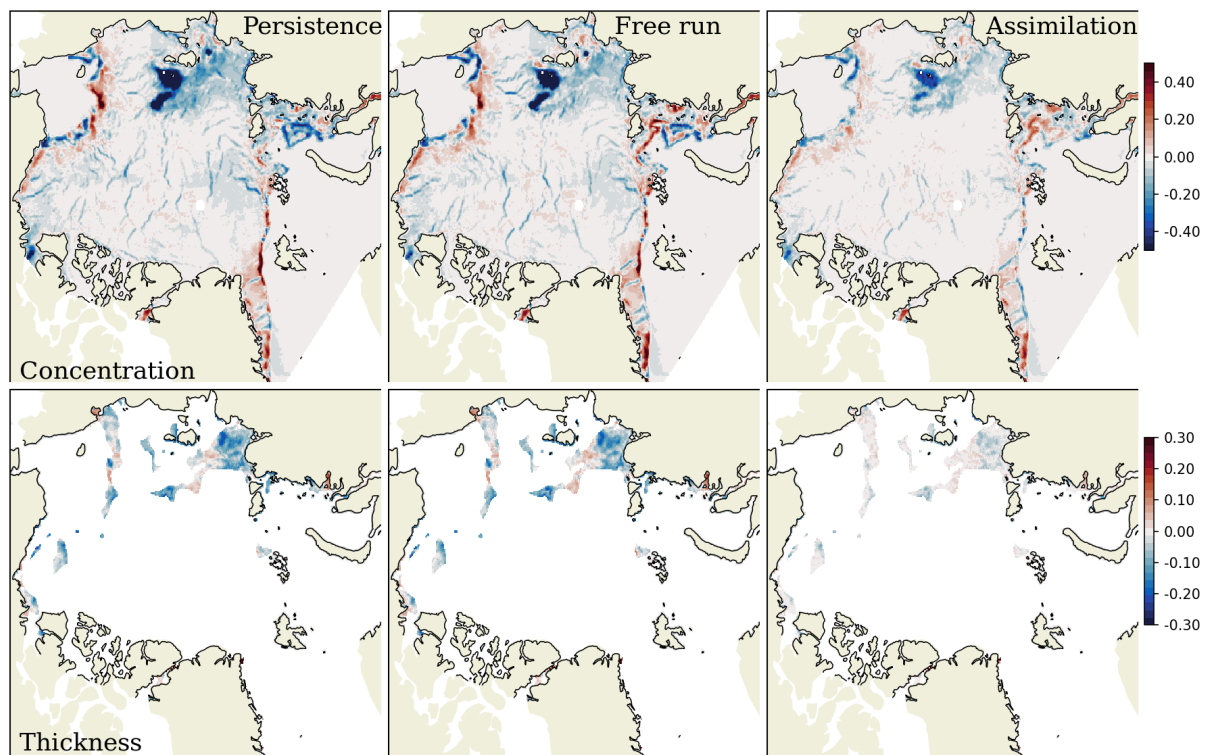
The Cryosphere
Discussions

Open Access

EGU

Figure 10. Maps of bias in concentration (upper row) and thin ice thickness (lower row) for 3 different cases: persistence, no assimilation, assimilation of SIC and SIT. The biases are averaged over 8 Nov 2019 - the first 24 hours after assimilation.

concentration (coloured lines on fig. 12, top) are close to the observations (black line, Figure 12, top) and stay well within the observational uncertainty (grey shaded area, Figure 12) not only during the period of rapid freeze-up (Nov–Dec) but also once ice growth has stabilised (Jan-Mar). The RMSE of concentration predictions on the first day (4th day) is around 4% (6%) with a slight negative bias of around -0.2 % (-5 %) (see Table 2). In November – February period the areas with negative bias (up to -20 %) of the concentration forecasts are predominantly located in the central Arctic. The ice edge in the Barents and Greenland seas is characterised by overestimation of ice concentration by $20 - 40$ %. In March – April sea ice concentration in the Barents Sea and Fram Strait are strongly underestimated with average negative bias in concentration of -2 %.

Sea ice extent predictions also closely follow observations: RMSE on the first day (4th day) does not exceed $10^5\,\mathrm{km}^2$ ($1.8 \times 10^5\,\mathrm{km}^2$) with overall a minor negative bias of $2–10 \times 10^4\,\mathrm{km}^2$ (see Table 2). Note the large improvement in extent from the free run (also see Table 1).

Thin ice thickness overestimates by the model are consistently higher than observations by $1 - 2$ cm on the first day of forecast and $3 - 5$ cm on the 4th day with RMSE growing from 7 to $10 - 14$ cm. Area of thin ice is considerably larger in November – December than in January – February.
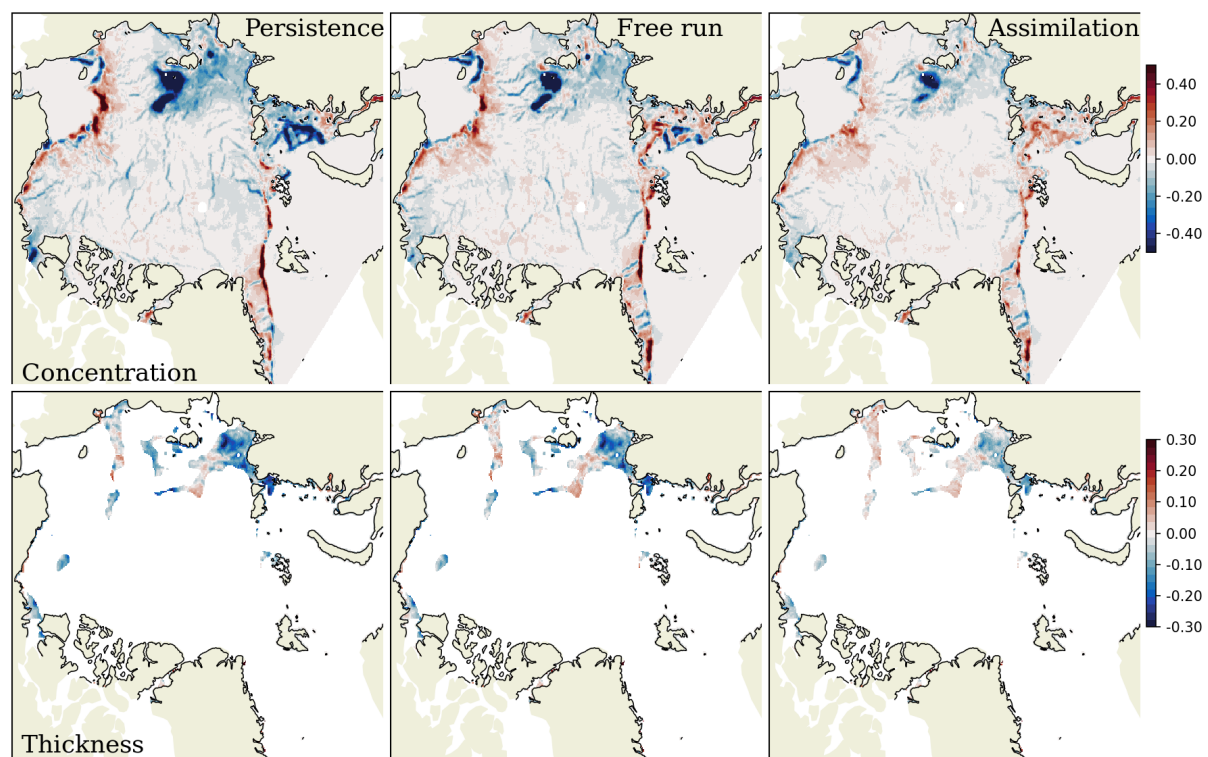
Figure 11. Maps of biases for 9 Nov 2019 - after 48 hours after assimilation (see caption of fig. 10 for details).

Ice drift is predicted with very high accuracy: RMSE for drifters placed on the first day at midday (recall the OSISAF drift product covers a 2-day period) is between 2.8 and 3.2 km/day on average; the VRMSE is slightly higher, ranging from 3.8 – 4.5 km/day. These values are about 0.5 km/day higher than for the free run (see Table 1), which used best estimates (i.e. the first day of each forecast forcing) for the atmospheric and ocean forcing; this part of the error is presumably largely due to error in the forecast winds (our forecasts use the full forecast forcing corresponding to the start day of our forecast). The RMSE and VRMSE do not show significant variations within the studied period from November 2018 to March 2019 and almost doesn't change during the first three days, implying the quality of the forecast drift is reasonably good for the first four days. There is a minor negative bias of -0.2 km/day for Nov-Dec and slight positive bias of $0.05 - 0.18$ km/day for Jan - Apr.

The RMSE and VRMSE in drifters placed on the fourth day is higher by about $1 - 1.5$ km/day, but the bias only increases by about 0.1 km/day. (For Nov-Dec, this actually makes it closer to zero.)

A map of forecast drift bias (see Figure 15) averaged over the entire period and for the first three days of forecast shows that the model underestimates eastward export of ice north of Greenland by $2 - 3$ km/day, underestimates anticyclonic drift in the Beaufort Gyre by $1 - 2$ km/day, overestimates the Transpolar Drift by $1 - 2$ km/day and overestimates westward drift in the Laptev sea by $3 - 5$ km/day.
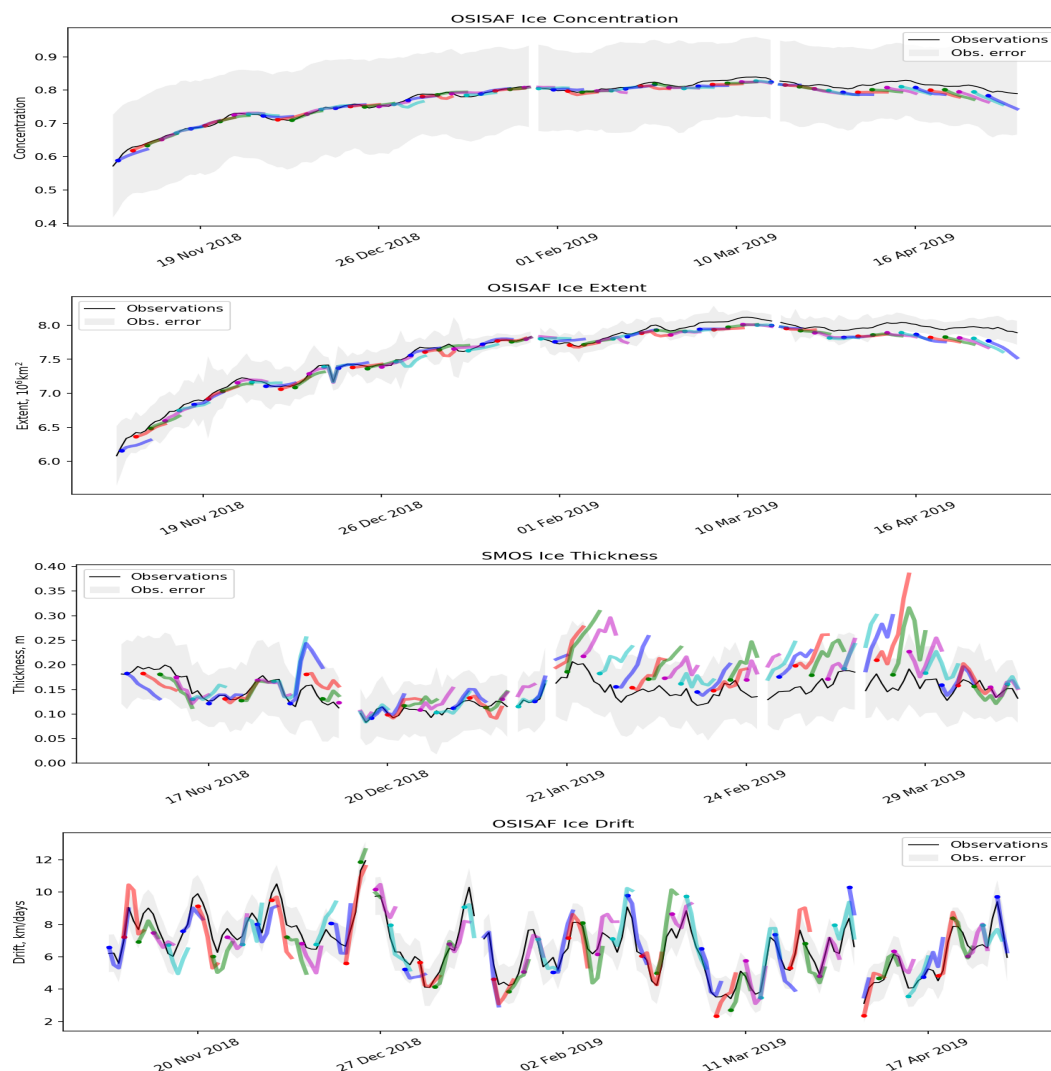
Figure 12. Time series of sea ice concentration, extent, thickness and drift averaged over ice covered waters from OSISAF and SMOS observations (black line) and forecasted by neXtSIM (coloured lines). Error-bars indicate the averaged uncertainty in the observations.
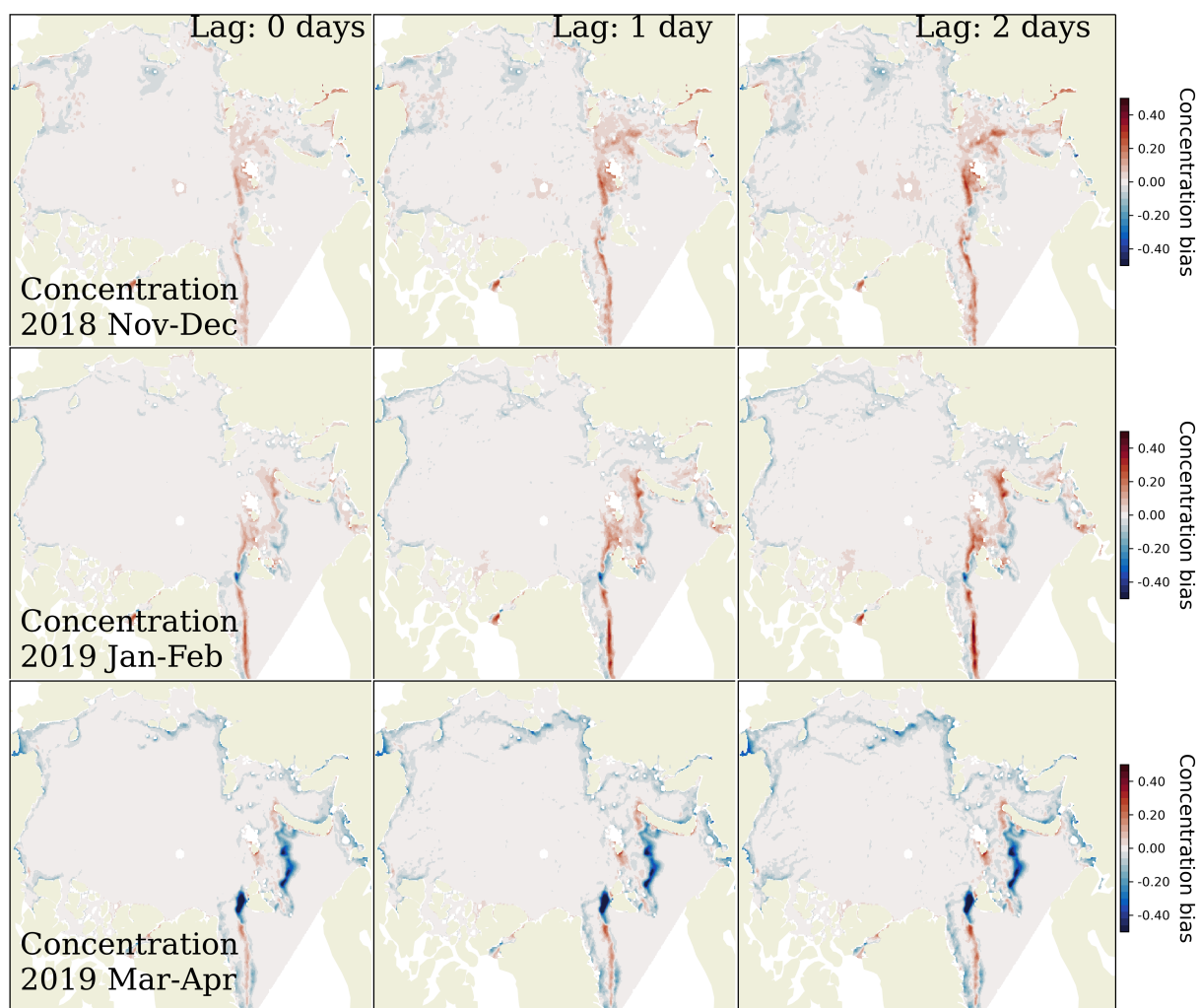
Figure 13. Maps of averaged biases in concentration for the first three days of forecast.
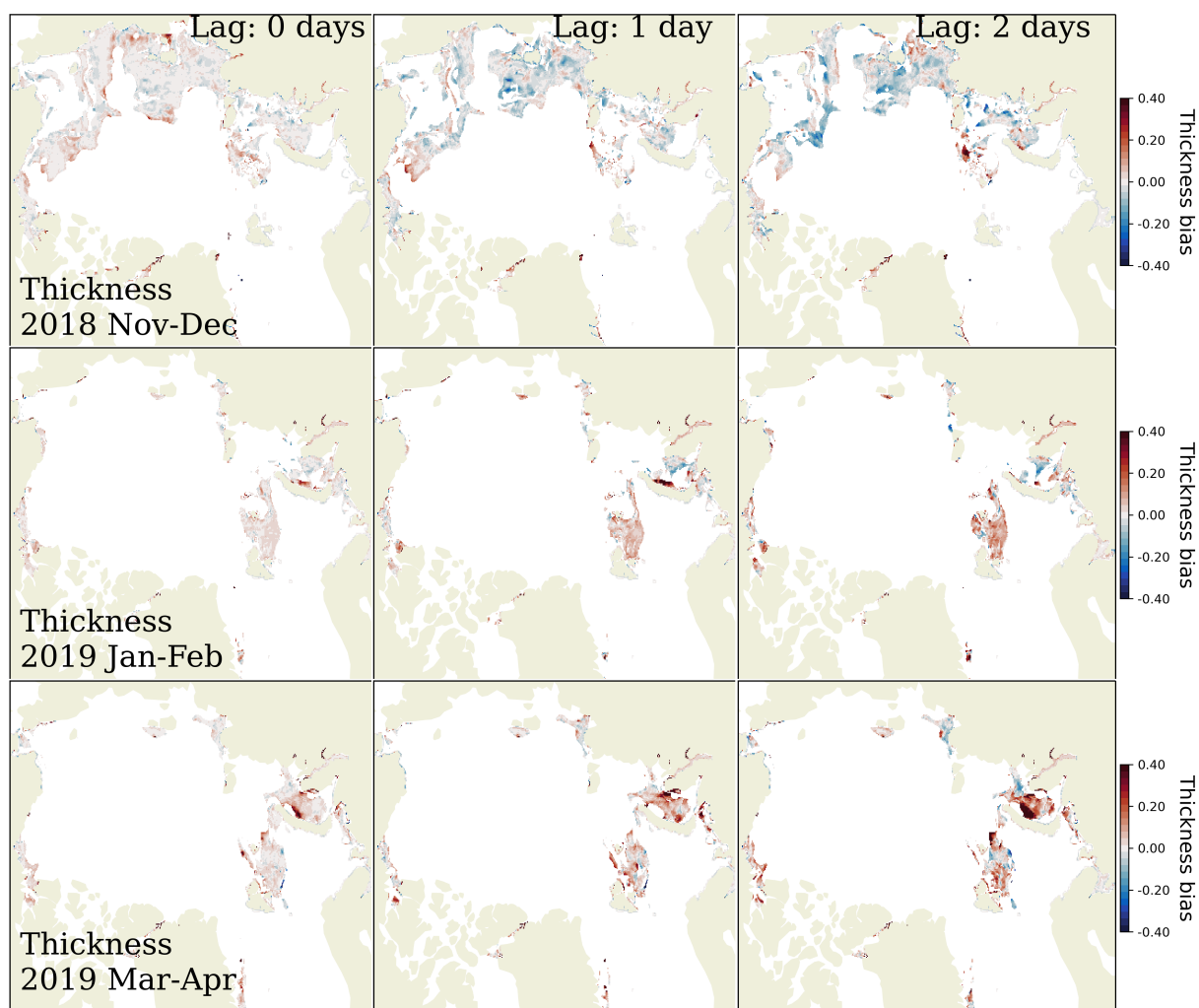
Figure 14. Maps of averaged biases in thin ice thickness for the first three days of forecast.
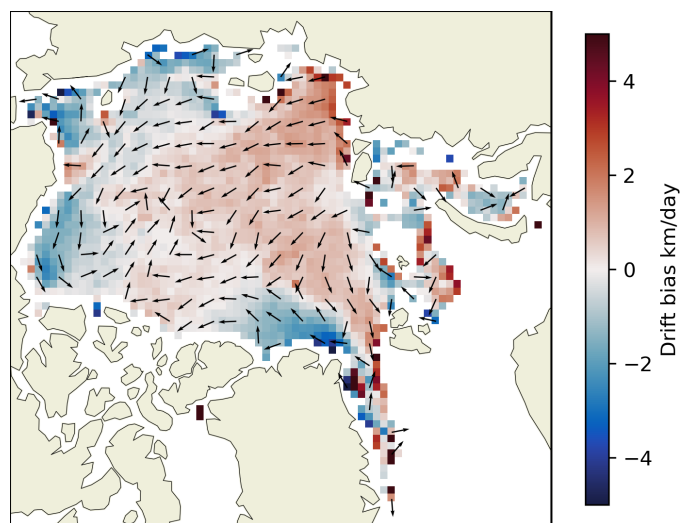
The Cryosphere
Discussions
EGU

Figure 15. Map of forecast drift bias (km/day) averaged over Nov 2018 to March 2019 for four first days of forecast.

Table 2. Accuracy of the scalar variables from the forecasts, with lead time of 1 day and 4 days. Concentration and extent are evaluated against OSISAF SSMI, thin ice thickness is evaluated against SMOS. The results are averaged over three periods: November – December, January – February and March – April.

		Bias		RMSE	
		1 day	4 days	1 day	4 days
	Nov-Dec	-0.19	-0.28	4.02	5.16
Concentration, %	Jan-Feb	-0.36	-0.55	3.16	4.17
	Mar-Apr	-1.30	-1.97	4.76	6.12
	Nov-Dec	-0.03	-0.04	0.09	0.15
Extent, $10^6 \mathrm{km}^2$	Jan-Feb	-0.02	-0.02	0.08	0.12
	Mar-Apr	-0.12	-0.14	0.15	0.18
	Nov-Dec	0.00	0.00	0.07	0.10
Thickness, m (thin ice only)	Jan-Feb	0.02	0.05	0.09	0.14
	Mar	0.02	0.05	0.09	0.13

Table 3. Accuracy of the drift from the forecasts, compared to the OSISAF drift product, with lead times of 1 day and 4 days. The results are averaged over three periods: November – December, January – February and March – April.

	Bias		RMSE		VRMSE	
	1 day	4 days	1 day	4 days	1 day	4 days
Nov-Dec	-0.24	-0.05	3.16	4.18	4.50	6.13
Jan-Feb	0.05	0.17	2.79	3.89	3.92	5.32
Mar-Apr	0.08	0.18	2.80	3.77	3.80	5.30

6 Discussion

For our free run, the model is consistently overestimating the ice extent compared to the OSISAF SSMI concentration and this dominates the error statistics of both concentration and thickness. There also seems to be a negative bias in the central Arctic which could have a number of origins: problems in forcing like the heat fluxes/air temperature; snowfall from forcing; problems with dynamics — too much export (discussed further below), or too little convergence, or too little opening (which would lead to too little new ice formation); problems with the snow cover. However, the total bias is quite close to zero. The average drift errors are relatively good overall, with the total RMSE $3.5 - 4.5$ km/day (being higher at the start of the winter). The main bias is in the Beaufort Sea where the model is consistently too slow, and the Laptev Sea where it is too fast. The drift in the Greenland Sea is consistently too fast, and the transpolar drift is also slightly too fast. This could be related to the overestimation in extent and also the thickness underestimation in the central Arctic.

Coming to the performance of the forecasts, there are several possible reasons why we observe overestimation of ice concentration and thin ice thickness by the model compared to satellite observations. First, the atmospheric forcing used both for the free run and the forecast may be underestimating air temperatures and, consequently increasing the heat loss from the ocean and concomitant growth of ice. Second, the passive microwave observations may be underestimating ice concentration especially in the vicinity of the ice edge where thin ice is dominating. At the same time SMOS observations of sea ice thickness close to the boundary with thick ice thickness can also be quite uncertain and underestimated. Finally, the displacement of ice into open waters due to slightly overestimated drift in the model can lead to mismatch of the ice edge position.

Apart from the errors in the forecast winds, the observed discrepancies in the drift forecasts could be caused by the following. North of Greenland the sea ice may be simulated as too packed and rigid, which prevents sufficient fragmentation and slows down the drift. In the Beaufort Sea it is known that the TOPAZ4 system underestimates the speed of the ocean currents and misplaces the center of the gyre. The Transpolar Drift could be being overestimated due to positive biases in the atmospheric forcing and overly strong winds, and the too-thin ice in the central Arctic could also be playing a role. In the Laptev Sea the extent of fast sea ice is underestimated by neXtSIM. This comes from the fact that in the model polynyas open closer to the shore and therefore sea ice detaches from the fast ice in the wrong location and drifts offshore from there — if compared to observations from satellite.

We also presented and assessed a novel method of nudging: we introduced some compensation for excessive heat flux due to reduction of concentration in assimilation, whereby the heat flux in the model out of the ocean (this is primarily to the atmosphere) is reduced according to observations of sea ice concentration. This improves our forecasts of sea ice concentration, thickness and extent, reducing errors which occur due to biased atmosphere or ocean forcing. Our experiments with the parameter n in (4) found that linear correction ($n = 1$) is not sufficient for the improvement due to assimilation to persist longer than $1 - 2$ days.

As written in the description section, running of the model requires relatively limited resources. That allows us to run the forecast system at high resolution and to cover the entire Arctic region. We use a workstation based on the AMD Ryzen Threadripper 2990WX CPU, which includes 32 cores being able to run at a base frequency clock speed of about 3.5 GHz. Our experiments show that running of a 7-day forecast for the entire Arctic ocean at 7.5 km resolution (each mesh triangle is covering approximately $50\,\text{km}^2$) takes approximately 22 min on 8 cores. Run time is proportional to the square of resolution (88 min for 3.5 km forecast) and decreases almost linearly with number of cores: 11.5 min for a 7.5-km forecast and 46 min for a 3.5-km forecast on 16 cores.

7 Conclusions and future directions

The neXtSIM-F forecast system has been tested for the northern winter of $2018 - 2019$ with different data being assimilated and has been found to perform well.

Despite drift not being assimilated in our system, we obtain fairly good agreement with observations, comparing well to the more sophisticated coupled ice-ocean forecast systems TOPAZ and GOFS. Notwithstanding different time periods and data used to assess the different forecast systems, the forecast sea ice drift by neXtSIM-F gives lower RMSE and VRMSE, and the bias remains close to zero over the whole period from Nov 2018 – Apr 2019. The forecasts using saved atmospheric and ocean forecasts as forcing have good agreement with observations, with only slightly higher errors than the free run for the first four days which uses best estimates for the ocean and atmospheric forcings.

The neXtSIM-F forecast system assimilates OSISAF sea ice concentration and SMOS sea ice thickness by modifying the initial conditions daily and adding a compensating heat flux to prevent removed ice growing back too quickly. This greatly improved the agreement of these quantities with observations for the first $3 - 4$ days of the forecast.

neXtSIM-F will become operational in November as part of the Copernicus Marine Environment Monitoring Services (CMEMS), and the next steps in the evolution of the system are first to assess the forecast performance for the spring and summer seasons, and to increase the resolution from about 7.5 km to about 3.5 km. The former task is a challenging one as passive microwave data becomes less reliable in summer and the SMOS sea ice thickness product is only available from October to April. Thus the data we have used in this study will either be less reliable or else unavailable outside these months. One possible alternative is to use ice charts — e.g. the United States Naval Ice Center[4] produces daily, pan-Arctic ice charts that could be used for correcting the ice extent. Other alternatives for assimilating extent are MASIE and IMS (used by GOFS:

---

[4]https://www.natice.noaa.gov/Main_Products.htm

see sec. 2) and automatic ice type classification from SAR (synthetic aperture radar): e.g. Zakhvatkina et al. (2017) presented an algorithm for processing Radarsat 2 SAR data, while an algorithm for processing Sentinel 1 SAR data under development at NERSC (Park et al., 2019) will also become operational in November 2019 and be distributed by CMEMS.

5   We also plan to test the benefits of assimilation of SAR-derived ice drift (Korosov and Rampal, 2017) on the system. The proposed approach would be to compute sea ice deformation rates from the observed SAR-derived drift and use this information to correct the damage field in the model. The expected outcome is to improve the location and timing of lead and ridge formation, as well as the large-scale drift pattern itself. A framework to produce an ensemble forecast with neXtSIM-F is also being developed (as a follow-up of the work of Rabatel et al., 2018), with the ultimate aim of using the Ensemble Kalman Filter (EnKF) assimilation method. Work on using EnKF with models running on adaptive meshes (like neXtSIM) is being

10   developed in parallel at NERSC (Aydoğdu et al., 2019).

Author contributions.   TW and AK wrote the paper and did the experiments. PR and EO contributed to writing and planning the paper and experiments. EO was also behind many background developments in the model code.

Competing interests.   No competing interests.

References

Aydoğdu, A., Carrassi, A., Guider, C. T., Jones, C. K. R. T., and Rampal, P.: Data assimilation using adaptive, non-conservative, moving mesh models, Nonlinear Processes in Geophysics Discussions, pp. 1–32, 2019.

Azzara, A. J., Wang, H., Rutherford, D., Hurley, B., and Stephenson, S. R.: A 10-year projection of maritime activity in the US Arctic region, Washington, DC: The International Council on Clean Transportation, pp. 163–178, 2015.

Bleck, R.: An oceanic general circulation model framed in hybrid isopycnic-Cartesian coordinates, Ocean Modelling, 4, 55–88, 2002.

Bouillon, S. and Rampal, P.: Presentation of the dynamical core of neXtSIM, a new sea ice model, Ocean Modelling, 91, 23–37, https://doi.org/10.1016/j.ocemod.2015.04.005, 2015.

Dansereau, V., Weiss, J., Saramito, P., and Lattes, P.: A Maxwell elasto-brittle rheology for sea ice modelling, The Cryosphere, 10, 1339–1359, 2016.

Drange, H. and Simonsen, K.: Formulation of air-sea fluxes in the ESOP2 version of MICOM, Tech. Rep. 125, Nansen Environmental and Remote Sensing Center, Thormøhlensgate 47, Bergen 5006, Norway, 1996.

Ek, M., Mitchell, K., Lin, Y., Rogers, E., Grunmann, P., Koren, V., Gayno, G., and Tarpley, J.: Implementation of Noah land surface model advances in the National Centers for Environmental Prediction operational mesoscale Eta model, J. Geophys. Res, 108, 8851, 2003.

Fetterer, F., Savoie, M., Helfrich, S., and Clemente-Colón, P.: Multisensor Analyzed Sea Ice Extent - Northern Hemisphere (MASIE-NH), Version 1, https://doi.org/doi.org/10.7265/N5GT5K3K, 2010.

Geuzaine, C. and Remacle, J.-F.: Gmsh: A 3-D finite element mesh generator with built-in pre- and post-processing facilities, International Journal for Numerical Methods in Engineering, 79, 1309–1331, https://doi.org/10.1002/nme.2579, https://onlinelibrary.wiley.com/doi/abs/10.1002/nme.2579, 2009.

Goessling, H. F. and Jung, T.: A probabilistic verification score for contours: Methodology and application to Arctic ice-edge forecasts, Quarterly Journal of the Royal Meteorological Society, 144, 735–743, https://doi.org/10.1002/qj.3242, https://rmets.onlinelibrary.wiley.com/doi/abs/10.1002/qj.3242, 2018.

Griffies, S., Harrison, M., Pacanowski, R., and Rosati, A.: A technical guide to MOM4, Tech. Rep. 5, Geophysical Fluid Dynamics Laboratory, NOAA, 2004.

Helber, R. W., Townsend, T. L., Barron, C. N., Dastugue, J. M., and Carnes, M. R.: Validation test report for the improved synthetic ocean profile (ISOP) system, part I: Synthetic profile methods and algorithm, Tech. rep., NAVAL RESEARCH LAB STENNIS DETACHMENT STENNIS SPACE CENTER MS OCEANOGRAPHY DIV, 2013.

Helfrich, S. R., McNamara, D., Ramsay, B. H., Baldwin, T., and Kasheta, T.: Enhancements to, and forthcoming developments in the Interactive Multisensor Snow and Ice Mapping System (IMS), Hydrological Processes: An International Journal, 21, 1576–1586, 2007.

Hunke, E. C. and Dukowicz, J. K.: An Elastic–Viscous–Plastic Model for Sea Ice Dynamics, J. Phys. Oceanogr., 27, 1849–1867, 1997.

Ivanova, N., Pedersen, L. T., Tonboe, R. T., Kern, S., Heygster, G., Lavergne, T., Sørensen, A., Saldo, R., Dybkjær, G., Brucker, L., and Shokr, M.: Inter-comparison and evaluation of sea ice algorithms: towards further identification of challenges and optimal approach using passive microwave observations, The Cryosphere, 9, 1797–1817, https://doi.org/10.5194/tc-9-1797-2015, https://www.the-cryosphere.net/9/1797/2015/, 2015.

Kaleschke, L., Tian-Kunze, X., Maaß, N., Beitsch, A., Wernecke, A., Miernecki, M., Müller, G., Fock, B. H., Gierisch, A. M., Schlünzen, K. H., Pohlmann, T., Dobrynin, M., Hendricks, S., Asseng, J., Gerdes, R., Jochmann, P., Reimer, N., Holfort, J., Melsheimer, C., Heygster, G., Spreen, G., Gerland, S., King, J., Skou, N., Søbjærg, S. S., Haas, C., Richter, F., and Casal, T.: SMOS sea ice prod-

uct: Operational application and validation in the Barents Sea marginal ice zone, Remote Sensing of Environment, 180, 264 – 273, https://doi.org/https://doi.org/10.1016/j.rse.2016.03.009, http://www.sciencedirect.com/science/article/pii/S003442571630102X, special Issue: ESA's Soil Moisture and Ocean Salinity Mission - Achievements and Applications, 2016.

5 Korosov, A. A. and Rampal, P.: A combination of feature tracking and pattern matching with optimal parametrization for sea ice drift retrieval from SAR data, Remote Sensing, 9, 258, https://doi.org/10.3390/rs9030258, http://www.mdpi.com/2072-4292/9/3/258, 2017.

Kurtz, N., Farrell, S., Studinger, M., Galin, N., Harbeck, J., Lindsay, R., Onana, V., Panzer, B., and Sonntag, J.: Sea ice thickness, freeboard, and snow depth products from Operation IceBridge airborne data, The Cryosphere, 7, 1035–1056, 2013.

Lavelle, J., Tonboe, R., Pfeiffer, H., and Howe, E.: Product User Manual for the OSI SAF AMSR-2 Global Sea Ice Concentration, Tech. Rep. SAF/OSI/CDOP2/DMI/TEC/265, Danish Meteorological Institute, http://osisaf.met.no/docs/osisaf_cdop2_ss2_pum_amsr2-ice-conc_

10 v1p1.pdf, 2016a.

Lavelle, J., Tonboe, R., Pfeiffer, H., and Howe, E.: Validation Report for The OSI SAF AMSR-2 Sea Ice Concentration, Tech. Rep. SAF/OSI/CDOP2/DMI/SCI/RP/259, Danish Meteorological Institute, http://osisaf.met.no/docs/osisaf_cdop2_ss2_valrep_ amsr2-ice-conc_v1p1.pdf, 2016b.

Lavelle, J., Tonboe, R., Jensen, M., and Howe, E.: Product user manual for osi saf global sea ice concentration, Tech. Rep.

15 SAF/OSI/CDOP2/DMI/SCI/RP/225, Danish Meteorological Institute, 2017.

Lavergne, T.: Validation and Monitoring of the OSI SAF Low Resolution Sea Ice Drift Product, Tech. Rep. SAF/OSI/CDOP/Met.no/T&V/RP/131, Norwegian Meteorological Institute, 2010.

Lavergne, T. and Eastwood, S.: Low Resolution Sea Ice Drift Product User's Manual, Tech. Rep. SAF/OSI/CDOP/met.no/TEC/MA/128, Norwegian Meteorological Institute, 2010.

20 Lavergne, T., Eastwood, S., Teffah, Z., Schyberg, H., and Breivik, L.-A.: Sea ice motion from low-resolution satellite sensors: An alternative method and its validation in the Arctic, Journal of Geophysical Research: Oceans, 115, 2010.

Marsan, D., Stern, H., Lindsay, R. W., and Weiss, J.: Scale dependence and localization of the deformation of Arctic sea ice, Phys. Rev. Lett., 93, 178 501, 2004.

Marshall, J., Hill, C., Perelman, L., and Adcroft, A.: Hydrostatic, quasi-hydrostatic and non-hydrostatic ocean modeling, J. Geophys. Res.,

25 102, 5733–5752, 1997.

Meier, W. N.: Losing Arctic sea ice: Observations of the recent decline and the long-term context, in: Sea Ice, edited by Thomas, D. N., chap. 11, pp. 290–303, John Wiley & Sons, 3 edn., 2017.

Melsheimer, C.: ASI Version 5 Sea Ice ConcentrationUser Guide, Tech. rep., 2019.

Melsom, A., Simonsen, M., Bertino, L., Hackett, B., Waagbø, G. A., and Raj, R.: Quality Information Document For Arctic Ocean Physi-

30 cal Analysis and Forecast Product ARCTIC_ANALYSIS_FORECAST_PHYS_002_001_A, Tech. Rep. CMEMS-ARC-QUID-002-001a, Norwegian Meteorological Institute, 2018.

Metzger, E., Helber, R. W., Hogan, P. J., Posey, P. G., Thoppil, P. G., Townsend, T. L., Wallcraft, A. J., Smedstad, O. M., Franklin, D. S., Zamudo-Lopez, L., and Phelps, M. W.: Global Ocean Forecast System 3.1 validation test, Tech. rep., NAVAL RESEARCH LAB STENNIS DETACHMENT STENNIS SPACE CENTER MS STENNIS SPACE . . . , 2017.

35 Onogi, K., Tsutsui, J., Koide, H., Sakamoto, M., Kobayashi, S., Hatsushika, H., Matsumoto, T., Yamazaki, N., Kamahori, H., Takahashi, K., et al.: The JRA-25 reanalysis, Journal of the Meteorological Society of Japan. Ser. II, 85, 369–432, 2007.

Overland, J. E., Hanna, E., Hanssen-Bauer, I., Kim, S.-J., Walsh, J. E., Wang, M., Bhatt, U. S., and Thoman, R. L.: Surface air temperature, in: Arctic Report Card 2018, NOAA, https://www.arctic.noaa.gov/Report-Card/Report-Card-2018, 2018.

Owens, R. G. and Hewson, T.: ECMWF Forecast User Guide, Tech. rep., ECMWF, Reading, https://doi.org/10.21957/m1cs7h, https://www.ecmwf.int/node/16559, <p> Replaces previous editions that were available as PDF documents.</p>, 2018.

Park, J.-W., Korosov, A. A., Babiker, M., Won, J.-S., Hansen, M. W., and Kim, H.-C.: Classification of Sea Ice Types in Sentinel-1 SAR images, The Cryosphere Discussions, 2019, 1–23, https://doi.org/10.5194/tc-2019-127, https://www.the-cryosphere-discuss.net/tc-2019-127/, 2019.

Parrish, D. F. and Derber, J. C.: The National Meteorological Center's spectral statistical-interpolation analysis system, Monthly Weather Review, 120, 1747–1763, 1992.

Perovich, D., Meier, W., Tschudi, M., Farrell, S., Hendricks, S., Gerland, S., Haas, C., Krumpen, T., Polashenski, C., Ricker, R., and Webster, M.: Sea ice, in: Arctic Report Card 2018, NOAA, https://www.arctic.noaa.gov/Report-Card/Report-Card-2018, 2018.

Rabatel, M., Rampal, P., Carrassi, A., Bertino, L., and Jones, C. K. R. T.: Impact of rheology on probabilistic forecasts of sea ice trajectories: application for search and rescue operations in the Arctic, The Cryosphere, 12, 935–953, https://search.proquest.com/docview/2014143795?accountid=8579, copyright - Copyright Copernicus GmbH 2018; Last updated - 2018-08-21; SubjectsTermNotLitGenreText - Arctic region, 2018.

Rampal, P., Weiss, J., Marsan, D., Lindsay, R., and Stern, H.: Scaling properties of sea ice deformation from buoy dispersion analysis, J. Geophys. Res., 113, https://doi.org/10.1029/2007JC004143, 2008.

Rampal, P., Bouillon, S., Ólason, E., and Morlighem, M.: neXtSIM: a new Lagrangian sea ice model, The Cryosphere, 10, 1055–1073, 2016.

Rampal, P., Dansereau, V., Ólason, E., Bouillon, S., Williams, T., and Samaké, A.: On the multi-fractal scaling properties of sea ice deformation, The Cryosphere Discussions, pp. 1–45, 2019.

Ricker, R., Hendricks, S., Kaleschke, L., Tian-Kunze, X., King, J., and Haas, C.: A weekly Arctic sea-ice thickness data record from merged Cryosat-2 and SMOS satellite data, Cryosphere, 11, 1607–1623, https://www.the-cryosphere.net/11/1607/2017/, 2017.

Saha, S., Moorthi, S., Wu, X., Wang, J., Nadiga, S., Tripp, P., Behringer, D., Hou, Y.-T., Chuang, H.-y., Iredell, M., Ek, M., Meng, J., Yang, R., Mendez, M. P., van den Dool, H., Zhang, Q., Wang, W., Chen, M., and Becker, E.: The NCEP Climate Forecast System Version 2, Journal of Climate, 27, 2185–2208, https://doi.org/10.1175/JCLI-D-12-00823.1, https://doi.org/10.1175/JCLI-D-12-00823.1, 2014.

Sakov, P. and Oke, P. R.: A deterministic formulation of the ensemble Kalman filter: an alternative to ensemble square root filters, Tellus A: Dynamic Meteorology and Oceanography, 60, 361–371, 2008.

Sakov, P., Counillon, F., Bertino, L., Lisæter, K. A., Oke, P. R., and Korablev, A.: TOPAZ4: an ocean-sea ice data assimilation system for the North Atlantic and Arctic, Ocean Science, 8, 633–656, 2012.

Samaké, A., Rampal, P., Bouillon, S., and Ólason, E.: Parallel implementation of a Lagrangian-based model on an adaptive mesh in C++: Application to sea-ice, J. Comp. Phys., 350, 84–96, https://doi.org/10.1016/j.jcp.2017.08.055, http://www.sciencedirect.com/science/article/pii/S0021999117306368, 2017.

Schweiger, A. J. and Zhang, J.: Accuracy of short-term sea ice drift forecasts using a coupled ice-ocean model, Journal of Geophysical Research: Oceans, 120, 7827–7841, https://doi.org/10.1002/2015JC011273, https://agupubs.onlinelibrary.wiley.com/doi/abs/10.1002/2015JC011273, 2015.

Semtner, A. J.: A model for the thermodynamic growth of sea ice in numerical investigations of climate, J. Phys. Oceanogr., 6, 379–389, 1976.

Simonsen, M., Hackett, B., Bertino, L., Røed, L. P., Waagbø, G. A., Drivdal, M., and Sutherland, G.: PRODUCT USER MANUAL For Arctic Ocean Physical and Bio Analysis and Forecasting Products ARCTIC_ANALYSIS_FORECAST_PHYS_002_001_A ARC-

TIC_ANALYSIS_FORECAST_BIO_002_004   ARCTIC_REANALYSIS_PHYS_002_003   ARCTIC_REANALYSIS_BIO_002_005,
Tech. Rep. CMEMS-ARC-PUM-002-ALL, Norwegian Meteorological Institute, 2018.

Stern, H. and Lindsay, R.: Spatial scaling of Arctic sea ice deformation, Journal of Geophysical Research: Oceans, 114, 2009.

Tian-Kunze, X., Kaleschke, L., Maaß, N., Mäkynen, M., Serra, N., Drusch, M., and Krumpen, T.: SMOS-derived thin sea ice thickness:
   Algorithm baseline, product specifications and initial verification, The Cryosphere, 8, 2014.

Tonboe, R. and Lavelle, J.: The EUMETSAT OSI SAF AMSR-2 Sea Ice Concentration Algorithm Algorithm Theoretical Basis Doc-
   ument, Tech. Rep. SAF/OSI/CDOP2/DMI/SCI/MA/248, Danish Meteorological Institute, http://osisaf.met.no/docs/osisaf_cdop2_ss2_
   atbd_amsr2-sea-ice-conc_v1p1.pdf, 2015.

Tonboe, R. and Lavelle, J.: Product user manual for osi saf global sea ice concentration, Tech. Rep. SAF/OSI/CDOP/DMI/SCI/MA/189,
   Danish Meteorological Institute, 2016.

Tonboe, R., Lavelle, J., Pfeiffer, R.-H., and Howe, E.: Product user manual for osi saf global sea ice concentration, Tech. Rep.
   SAF/OSI/CDOP3/DMI_MET/TEC/MA/204, Danish Meteorological Institute, 2016.

Wessel, P. and Smith, W. H. F.: A global, self-consistent, hierarchical, high-resolution shoreline database, Journal of Geophysical Research:
   Solid Earth, 101, 8741–8743, https://doi.org/10.1029/96JB00104, https://agupubs.onlinelibrary.wiley.com/doi/abs/10.1029/96JB00104,
   1996.

Winton, M.: A Reformulated Three-Layer Sea Ice Model, J. Atmos. Ocean Tech., 17, 525–531, 2000.

Zakhvatkina, N., Korosov, A., Muckenhuber, S., Sandven, S., and Babiker, M.: Operational algorithm for ice–water classification on
   dual-polarized RADARSAT-2 images, The Cryosphere, 11, 33–46, https://doi.org/10.5194/tc-11-33-2017, https://www.the-cryosphere.
   net/11/33/2017/, 2017.

Zygmuntowska, M., Rampal, P., Ivanova, N., and Smedsrud, L. H.: Uncertainties in Arctic sea ice thickness and volume: new estimates and
   implications for trends, The Cryosphere, 8, 705–720, 2014.